ADVANCED SUSTAINABLE SYSTEMS
www.advsustainsys.com

Graphene Nanoplatelets/Barium Titanate Polymer Nanocomposite Fibril: A Remanufactured Multifunctional Material with Unprecedented Electrical, Thermomechanical, and Electromagnetic Properties

Raghvendra Kumar Mishra, Saurav Goel, Iva Chianella,* and Hamed Yazdani Nezhad**

A novel, zero-waste and recycling plastic waste solution is introduced, to scalably produce graphene nanoplatelets/barium titanate (GNP/$BaTiO_3$) polymer nanocomposite fibrils. A comprehensive investigation is performed to evaluate the compatible and non-compatible recycled polypropylene (PP)/polyethyleneterephthalate (PET) blends combined with functional (electrical, piezoelectric,and dielectric) materials for in-situ fibril production. The nanocompositefibrils made from recycled PP, PET and GNPs/$BaTiO_3$ with high-aspect ratio disparity (400:1) are produced, which exhibit significantly enhanced electrical, thermomechanical, and electromagnetic characteristics. Single-screw extrusion is utilised to fabricate the fibrils with the in-situ fibril morphology of PET and GNPs/$BaTiO_3$ leading to improved electrical conductivity. It is demonstrated that such fibril morphology restricts the chain mobility of polymer molecules, and ultimately increases viscosity and strain energy. Moreover, the study demonstrates a positive reinforcement effect from the utilisation of PET fibrils and GNPs/$BaTiO_3$ in a PP matrix, dominated by the high-aspect ratio, stiffness, and thermal stability of GNPs/$BaTiO_3$. Furthermore, it is observed that the mechanical properties and tension-bearing capacity of the PP are significantly improved by such incorporation. The study also demonstrates that the protection of the remanufactured nanocomposites against electromagnetic interference is significantly improved with the increasing GNPs/$BaTiO_3$ content and the morphological transition from spherical to fibril-shaped PET.

1. Introduction

One of the most important environmental problems of the current time is plastic waste. Nearly eight million tons of plastic waste enters oceans each year which causes substantial irreversible damage to the marine ecosystem.[1] It has become one of the planet's most visible and pervasive forms of pollution, with disastrous consequences to living beings and the environment. Plastic waste pollutes water and soil, as well as deteriorates wildlife and causes significant damage to the environment.[2] The negative effects of plastic trash on the environment make it a top priority to find innovative ways to or eliminate it or significantly mitigate it.[3] Conductive polymer nanocomposites offer a viable and promising solution to many of today's technological problems[2,4]; however, only one type of polymer is currently recyclable at large scale with minimal carbon footprint associated with its process, i.e., relatively low-melt temperature thermoplastics. Nature based (natural and bio-) polymers still have a long way to be adopted for large

R. K. Mishra, I. Chianella
School of Aerospace
Transport and Manufacturing
Cranfield University
Cranfield MK43 0AL, UK
E-mail: i.chianella.1998@cranfield.ac.uk

S. Goel
School of Engineering
London South Bank University
London SE1 0AA, UK
E-mail: goels@lsbu.ac.uk

S. Goel
Department of Mechanical Engineering
University of Petroleum and Energy Studies
Dehradun 248007, India

H. Yazdani Nezhad
Advanced Composites Research Group
School of Science and Technology
City, University of London
London EC1V 0HB, UK
E-mail: h.yazdaninezhad@leeds.ac.uk

The ORCID identification number(s) for the author(s) of this article can be found under https://doi.org/10.1002/adsu.202300177

DOI: 10.1002/adsu.202300177

scale and mass production for public use. One potential and immediate solution to tackle the current plastic waste issue is by recycling current plastic wastes into new products which open up opportunities for new materials development such as multifunctional polymer composites, e.g., electrically conductive polymers can be remanufactured from mixing plastic waste with functional conductive particles. Amongst these, conductive polymer nanocomposites have several advantages over traditional materials.[5] The nanocomposites combine the functional and structural properties of nanomaterials and polymers for benefiting traceability, properties tailoring and recyclability,[2,4] with emerging applications in electronics, energy storage, biomedical devices, and automotive parts.[6–11] On the other hand, immiscible polymer blend-based nanocomposites are particularly appealing because they offer characteristics that traditional composites do not. Blends of immiscible polymers contain two or more polymers that do not mix but instead generate distinct phases in a composite material, that enables the development of various immiscible polymer blend-based nanocomposites. Fundamentally, the performance of polymer blend-based composites and nanocomposites is underpinned by the blended microstructure, its morphological features and filler dispersion,[12] providing a control over parts remanufacture out of blend combinations, which again benefit sustainable developments. Such blends are being used in an increasing number of applications due to their superior mechanical, thermal, and electrical properties when compared to non-composite polymers. Their microstructure can be tailored via dispersion of functional fillers such as nanoparticles, carbon nanotubes (CNT), or graphene, which may greatly influence the performance of resulting final blends,[13] despite the challenge of achieving strong filler-polymer adhesion, and compatibility within blending components.[14] Several experiments have been carried out to produce compatible, electrically conductive polymer nanocomposites via combining novel process techniques and nano-scale functional fillers into immiscible polymer blends. The main challenge has been to find a way to incorporate these nano-scale fillers into immiscible polymer blends to create compatible and stable electrically conductive composites.[15] This owes to the fact that conductive nanocomposites often exhibit excellent conductivity,[16] high stiffness,[17] heat resistance,[18] decreased gas permeability[19] and superior electromagnetic interference (EMI) shielding properties compared to those in neat polymer or immiscible polymer blends.[20]

Conductive fillers used in conjunction with composites (such as fiber-reinforced thermoplastic composites) or polymer blends can improve the electrical, thermal, and mechanical performance, broadening the potential for generating micro-fiber composites (FC).[21,22] For this purpose, a variety of carbon-based materials can be used as reinforcement and/or conducting fillers including carbon black,[23] single-walled CNT,[24] multi-walled CNT,[25] carbon nanofibers (CNFs), graphene nanoplatelets (GNPs)[26] in a variety of polymer matrices. Due to their optimal polymer-compatibility, recyclability, and low-cost processability, these composites have been employed in many industrial applications. There is also a high demand for electrically conductive polymer composites that fulfill the performance standards required in electronics,[27] EMI shielding,[28] and other applications.[29–31] Such performance is influenced by a variety of parameters, including particulate and fibril morphologies suggesting numerous combinations of blends/composites/nanocomposites, and/or nanofiller dispersion and distribution.[30,32–36]

Additionally, there is indeed a high demand for low electrical percolation threshold in polymer composite materials.[37] The electrical percolation threshold is an essential parameter in polymer composites, which indicates the minimum concentration of conductive fillers required to generate a continuously conductive network. Nanofillers such as graphene, due to their small size and high surface energy, often form in agglomerates, making the creation of a continuous conducting network at lower concentrations challenging However, a low electrical percolation threshold is beneficial since it requires a smaller concentration of nanofillers, allowing for the composite material to maintain its mechanical properties, while achieving the desired electrical conductivity, thus resulting in low energy requirements for material processing and low costs. Thus, having a low electrical percolation threshold is particularly advantageous for composite materials that require both high electrical conductivity and thermomechanical properties.[38,39] Another crucial issue to consider in waste management is sustainability and recyclability. Microbeads, for instance, are a type of plastic waste that can harm marine life and the environment. To reduce the negative impact of plastic waste on marine ecosystems, natural alternatives such as salt, sugar, or crushed fruit kernels can replace plastic microbeads. Additionally, sustainable waste management measures, such as recycling, can help reduce plastic waste buildup in landfills and seas. Some materials, such as polypropylene, polyethylene terephthalate, and nanofillers like GNPs and barium titanate ($BaTiO_3$) can be recycled at minimal production temperature, energy, emission, and costs. If this is realized and quantified for large scale, it would add to prioritizing sustainability and recyclability in plastic waste management and reduce the harm caused by microbeads on marine ecosystems.[40,41]

Graphene Nanoplatelets (GNPs) and Barium Titanate ($BaTiO_3$) are combined to produce high-performance composites with various applications. These composites offer improved mechanical properties such as improved strength and stiffness, electrical conductivity for applications[42–44] such as sensors and electronics, enhanced dielectric properties for capacitors and energy storage devices, and good compatibility with polymer matrices, enabling their use in diverse fields including aerospace, automotive, electronics, energy, and more.[45] Additionally, polymer blend composites have been investigated as a solution to mitigate microwave radiation pollution and enhance EMI shielding performance.[30,46] The aforementioned papers highlight the importance of selective confinement or dispersion of nanofillers in specific phases of the blend to improve composite properties. One of the literature study focused on polystyrene (PS)/ethylene-co-methyl acrylate (EMA) blends, demonstrating that confining carbon nanotubes and carbon nanofibers in the EMA phase significantly reduced the electrical percolation threshold, resulting in improved microwave absorb-

H. Yazdani Nezhad
School of Mechanical Engineering
Faculty of Engineering and Physical Sciences
University of Leeds
Leeds LS2 9JT, UK

ing properties.[47] Another study explored EMA/thermoplastic polyolefin (TPO) blends, showing that preferential distribution of carbon particles in the EMA phase led to excellent EMI shielding performance at low filler loading.[48] Carbon black reinforcement in a polystyrene/EMA blend enhanced EMI shielding performance.[49] Lastly, a solution mixing technique was employed to create lightweight blend composite films with improved electrical properties, thermal conductivity, and microwave shielding performance.[50] These studies collectively emphasize the potential of polymer blend composites in addressing microwave radiation pollution and enhancing EMI shielding in various applications. The incorporation of fibrils morphology and the combination of GNPs and $BaTiO_3$ in composites based on recycled plastic offers a synergistic effect. This approach addresses the microbead problem by utilizing recycled plastic instead of virgin materials. The enhanced mechanical properties and functionality of these composites contribute to sustainability efforts by promoting the reuse of plastic waste and reducing the environmental impact associated with microbead pollution.[51,52]

In this work, we have exploited such realization for scalability by investigating recycled polypropylene (PP)/Polyethylene terephthalate (PET) blended with GNPs/$BaTiO_3$ to obtain conductive composite blends and in situ fibrils-based composites, whose electrical, thermomechanical, and EMI properties were then quantified. The main objective of this work was to propose a remanufactured multifunctional composite based on fibrils reinforced in situ polymer composites with blended and recycled plastics. The resulting material aims to substitute current polymer blends and polymer nanocomposites based on the p-products, meeting their specific property requirements while achieving low percolation thresholds and favorable mechanical, electrical, and thermal features. It has been observed that the proposed composites in the fibrilform exhibit superior electrical, thermomechanical, and electromagnetic shielding properties, and a greater reinforcing impact than the particles-based blended nanocomposites. This would suggest a remanufactured and property-enhanced material system with a low percolation threshold, excellent electrical conductivity, thermal, mechanical, and electromagnetic shielding properties capable of benefiting a variety of multi-functional and recyclable materials and applications.

2. Experimental Section

The polymers were extruded using a single-screw Noztek filament extruder. Recycled polypropylene (acquired from PP bottles with average molecular weight of 500 000 g mol^{-1} and average density of 907.5 kg m^{-3}) employed in this study had a melt flow index (MFI) of – 11.0 g/10 min, as well as melting and glass transition temperatures of 167 and −10 °C, respectively (measured by differential scanning calorimetry, DSC). As an attempt to acquire a relatively large-scale laboratory container, the melt-flow index (MFI) of recycled polypropylene was tested in a 2.1 kg batch at a fixed temperature of 200 °C at 10 rpm in a single screw nozzle filament extruder. The MFI of recycled polyethylene terephthalate bottles was determined using a Noztek filament extruder within a 500 g recycled polyethylene terephthalate batch with a fixed temperature profile at 240 °C (acquired from PET bottles with average molecular weight of 35 000 g mol^{-1}, average density of 1370 kg m^{-3}). DSC was used to calculate the melting and crystallization temperatures of recycled polypropylene and polyethylene terephthalate. To introduce high-performance functional properties, the GNPs and BaTiO3 powders with specifications of 2.0–2.25 g cm^{-3} for Graphene platelets (GNPs) and average particle size < 2 μm for BaTiO3 were supplied by Sigma-Aldrich. They were mixed in the blend without any modification, and both had a thickness in a few nanometers. Additionally, the density of GNPs and BaTiO3 was 6.08 g mL^{-1} and 250 °C, respectively. The GNPs had an aspect ratio of nearly 400, while BaTiO3 had an aspect ratio of 1. Both Graphene platelets (GNPs) and BaTiO3 had a thickness in a few nanometers, with average particle sizes of < 2 and < 3 μm, and densities of 2–2.25 and 6.08 g mL^{-1} at 250 °C, respectively.

2.1. Processing of GNPs and $BaTiO_3$ Mixture

In a beaker, the solvents chloroform and acetone were mixed in a 2:1 ratio. The beaker was placed on the magnetic stirrer, and equal amounts of GNPs and $BaTiO_3$ were measured and added. To avoid solvent evaporation, the beaker was securely covered. The beaker was then heated at 50 °C for 60 min while magnetically stirred to produce a mixture of GNPs and $BaTiO_3$, after which sonication was performed to obtain a uniform dispersion of the nanomaterial's mixture in the solvent. The combination was then heated until dried out in a vacuum oven for 8 h at 80 °C, as illustrated in **Figure 1**, which highlights the methodology used for remanufacture of the multifunctional nanocomposites.

2.2. Processing of (polypropylene/polyethylene terephthalate) Blends

Before melt mixing, recyclable polypropylene and polyethylene terephthalate were pre-heated in a vacuum oven for 8 h at 80 °C. Melt mixing was then performed using a single screw Noztek filament extruder at 230 °C and 10 rpm to achieve a fixed weight ratio of 85/15. The extruded strands were crystallized using the air chilling process before being hot-pressed at a pressure of 10 MPa at 180 °C for 5 min, as illustrated in **Figure 2**a.

2.3. Preparation of GNPs and $BaTiO_3$ Based Nanocomposites (GBNC)

Initially, recycled polypropylene, recycled polyethylene terephthalate, GNPs, and $BaTiO_3$ mixtures were vacuum dried for 8 h at 100 °C. Recycled polypropylene, recycled polyethylene terephthalate, GNPs, and $BaTiO_3$ mixes were produced utilizing a single screw Noztek filament extruder. The needed quantities of GNPs and $BaTiO_3$ mixes were calculated as phr (parts per hundred matrix) of total fixed amounts of polypropylene and polyethylene terephthalate (85/15 ratio). The mixing was conducted at 230 °C and 10 rpm. The air-cooling process was used to crystallize the extruded strands. The crystalline strands were then hot-pressed for 5 min at 180 °C at a pressure of 10 MPa, as shown in Figure 2b, while their formulation and designation is reported in **Table 1**.

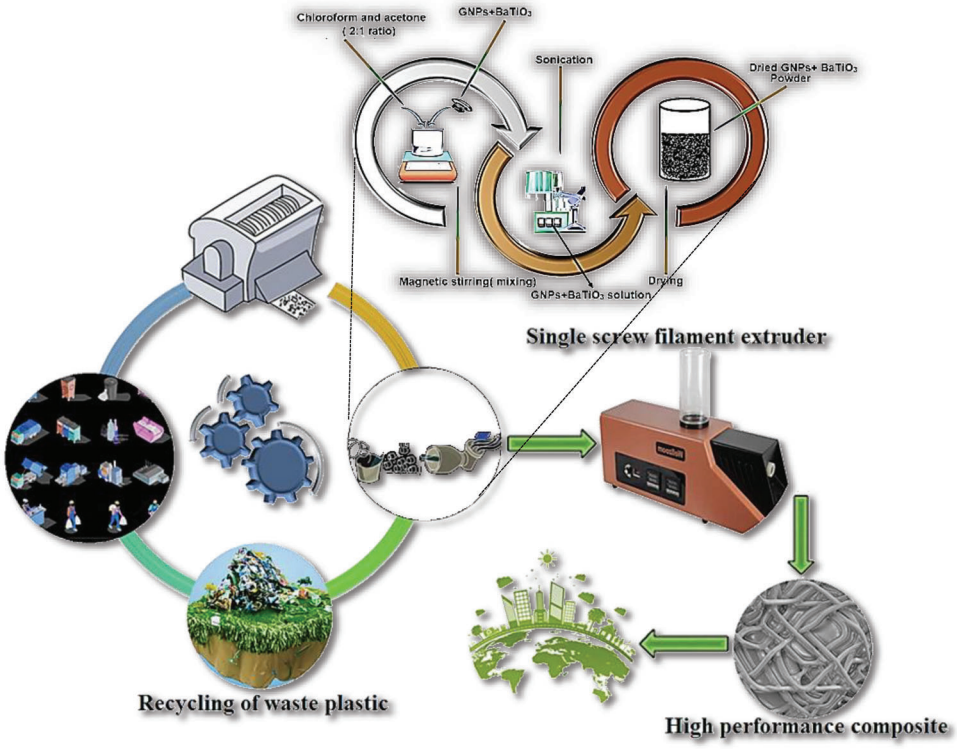

Figure 1. Proposed preparation methodology for remanufacturing high-performance multifunctional nanocomposite fibrils out of recycled polymer blends (herein PP/PET) and high-aspect-ratio functional nanosystems (herein GNPs/$BaTiO_3$).

2.4. Preparation of In Situ Fibrils-Based Composites (FC)

Recycled polypropylene and polyethylene terephthalate in situ fibrils composites were produced using a single-screw Noztek filament extruder and drawing process at an 85/15 fixed weight ratio (wt.%). Before using the single screw Noztek filament extruder and drawing process, recycled polypropylene and polyethylene terephthalate were heated in a vacuum oven for 8 h at 80 °C. Following drying, the recycled polymers were extruded in the form of strands at 230 °C at 10 rpm, followed by air cooling and drawing. The drawing was conducted at several draw ratios, but the drawing ratio of 8 was chosen to give optimal production quality, as described in the next section. The pulled strands were hot-pressed for 5 min at 180 °C (below the melting point of polyethylene terephthalate to maintain the in situ polyethylene terephthalate fibrils), as illustrated in **Figure 3**a.

2.5. Preparation of GNPs and $BaTiO_3$ Based Fibrils Nanocomposites (GBFNC)

Initially, recycled polypropylene, recycled polyethylene terephthalate, GNPs, and $BaTiO_3$ mixtures were vacuum dried for 8 h at 100 °C. Using the single screw Noztek filament extruder, various compositions of recycled polypropylene, recycled polyethylene terephthalate, GNPs, and $BaTiO_3$ mixtures were produced. The required GNPs and $BaTiO_3$ mixes were measured as phr of total fixed content of polypropylene and polyethylene terephthalate (85/15 ratio), as shown in **Table 2**. The mixing was done at

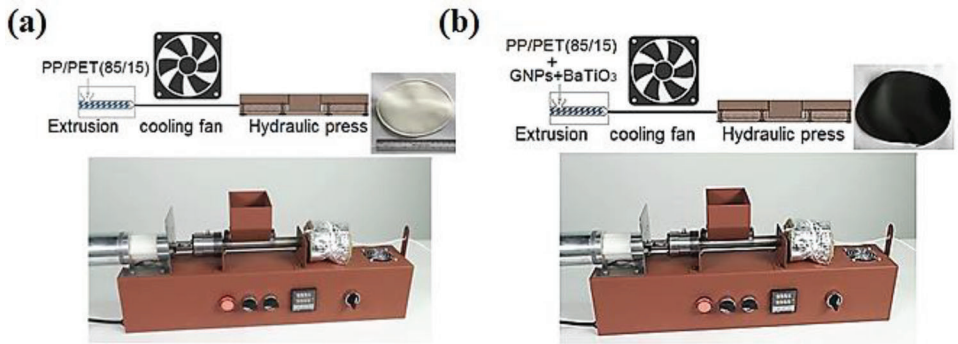

Figure 2. a) The exploratory setup for blends(B), b) Experimental setup for GNPs and $BaTiO_3$ based nanocomposites (GBNC).

Table 1. Formulation of GNPs and $BaTiO_3$-based nanocomposites and sample designation.

Samples	GNPs(Phr)	$BaTiO_3$ (Phr)	Designation
PP- polyethylene terephthalate (85% & 15%)	–	–	B
PP- polyethylene terephthalate (85 & 15 wt.%) /GNPs- $BaTiO_3$		1(phr)	(GBNC1)
PP- polyethylene terephthalate (85 & 15 wt.%) /GNPs- $BaTiO_3$		2(phr)	(GBNC2)
PP- polyethylene terephthalate (85 & 15 wt.%) /GNPs- $BaTiO_3$		3(phr)	(GBNC3)

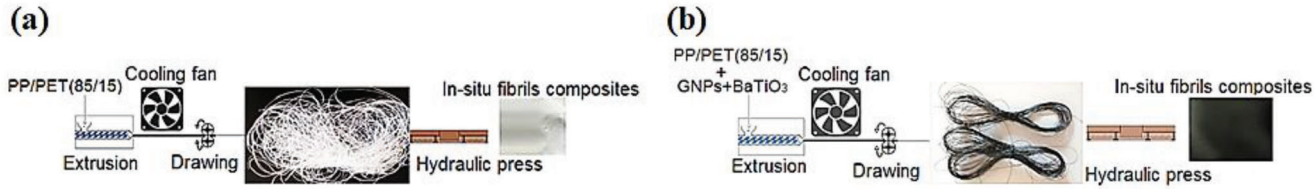

Figure 3. a) Morphology of the in situ fibrils microfibrillar composites (FC), b) Schematic representation of the experimental setup for GNPs and $BaTiO_3$ based in situ fibrils nanocomposites (GBFNC).

230 °C and 10 rpm. Air cooling crystallized the extruded strands before being drawn at various draw ratios. As demonstrated in **Figure 4**, through careful experimentation, it was determined that a drawing ratio of 8 resulted in the optimal conductivity, with an adequate fibrillar zone and enhanced physical properties that were greater than those physical properties with draw ratio of 2. It was observed that at ratios beyond 8, the conductivity level nearly saturates. The drawn strands were hot-pressed for 5 min at 180 °C (below the melting point of polyethylene terephthalate to retain the in situ polyethylene terephthalate fibrils), as illustrated in Figure 3b.

2.6. Characterization

2.6.1. Theoretical Study of Orientation Parameter During Drawing for In Situ Fibrils Composites and Nanocomposites

The amorphous and crystalline orientation parameters were utilized to estimate the degree of orientation of the amorphous and crystalline components, as well as the formation of fibrils.[53,54] The deformation configuration relevant for measuring the degree of stiffness and aspect ratio of fibrils during the drawing process is assumed to be the degree of orientation of the polymer's amorphous-crystallite phase. The orientation parameters were measured using the amorphous and crystalline orientation models at a drawing ratio of 8, where A_i = Area of undrawn strands, A_f = Area of drawn strands during drawing, as illustrated in Equations (1) and (2). The crystalline orientation parameter (*COP*) is given by:

$$\mathrm{COP} = 0.5\left[\frac{2\times\left(\frac{A_i}{A_f}\right)^3+1}{\left(\frac{A_i}{A_f}\right)^3-1}-\left(\left[\frac{3\times\left(\frac{A_i}{A_f}\right)^3}{\left(\left(\frac{A_i}{A_f}\right)^3-1\right)^{\frac{3}{2}}}\right]\times arctan\left(\left[\left(\left(\frac{A_i}{A_f}\right)^3-1\right)^{\frac{1}{2}}\right]\right)\right] \quad (1)$$

while the amorphous orientation parameter (*AOP*) is given by:

$$\mathrm{CAOP} = \frac{1}{5N}\times\left(\left(\frac{A_i}{A_f}\right)^2-\frac{1}{\left(\frac{A_i}{A_f}\right)}\right) \quad (2)$$

For all drawn samples, the orientation parameters were computed using a fixed draw ratio of 8. **Figure 5**a,b shows that when the nanofiller concentration increases, the crystallites and amorphous orientation parameters decrease due to the stiffness agglomeration and viscosity induced effects from the nanofillers in the polymer system. The changes in crystallite and amorphous chain orientation parameters are the results of the fillers' impact on the orientation of the polyethylene terephthalate crystallites lamella and amorphous chain when drawing. During drawing, an axial elongational force causes mechanical strain that affects the orientation of the amorphous chain and crystalline lamella, exhibiting a difference in fibril shape in in-situ fibrils composites and in situ fibrils nanocomposites (GBFNC). The polymer system's variation with nanofiller concentration results in

Table 2. Formulation of GNPs and $BaTiO_3$ based in situ fibrils nanocomposites.

Samples	GNPs(Phr)	$BaTiO_3$ (Phr)	Designation
PP- polyethylene terephthalate (85 &15 wt.%)	–	–	FC
PP- polyethylene terephthalate (85 & 15 wt.%) /GNPs- $BaTiO_3$		1(phr)	(GBFNC1)
Polypropylene – polyethylene terephthalate (85 & 15 wt.%) /GNPs- $BaTiO_3$		2(phr)	(GBFNC2)
Polypropylene – polyethylene terephthalate (85 & 15 wt.%) /GNPs- $BaTiO_3$		3(phr)	(GBFNC3)

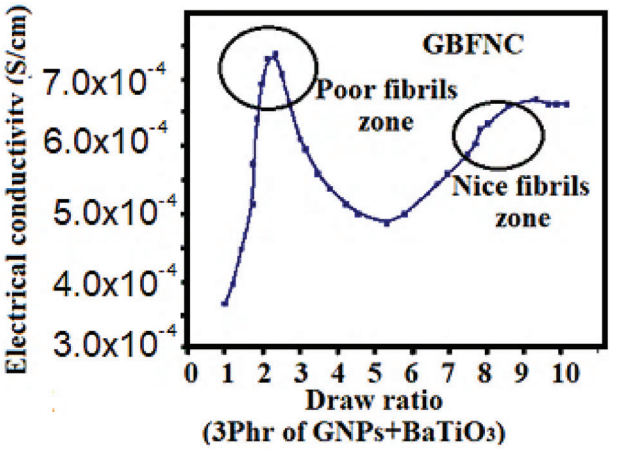

Figure 4. The variation of the electrical conductivity of GBFNC with draw ratio.

increased stiffness and viscosity. The draw ratio used is insufficient in the presence of nanofillers to distort and orient the amorphous chain and crystalline lamella inside the extruded strands. This is demonstrated by a considerable reduction in the orientation characteristics of amorphous and crystallite lamella in in-situ fibrils with nanofiller concentration. The semicrystalline polymer is made up of two regions: amorphous and lamellar (crystalline). An axial force is generated in the amorphous zone during the drawing. The shape of tiny fibril coalescence is closely connected to the stress generated in the amorphous area as well as lamella alignment. As the nanofiller concentration increases, the stress decreases in this location, as seen in Figure 5c. The nanofillers withstand the axial load at higher capacity due to possessing higher mechanical properties than the polymer, and mitigate the level transmitted to the polymer. The angle of the orientation graph for all samples indicates a rather similar trend. Figure 5d shows the angle of orientation of the polymer chain in the drawn state with respect to the undrawn state, and this relationship is approximated using the following Equation (3) [55,56];

$$tan\theta = \left(\left(\frac{A_i}{A_f}\right)^{\frac{-3}{2}}\right) \times tan\theta' \tag{3}$$

where θ' is the polymer chain's orientation angle before drawing, θ is the orientation angle after drawing, A_i is the area of undrawn extruded strands, which is simplified to be $(\pi d_i^2)/4$. We assume that all the samples were in the same state before drawing; therefore, we use the same $tan\theta'$ value for all the samples.[57] The ratios of orientation angles of drawn state to undrawn state ($tan\theta/tan\theta'$), were noticeably diversified across the samples. As predicted, the values and curves for the ratio of orientation angles of the drawn state decreased as the nanofillers concentration decreased. The fibril composite (FC) ratio near 0.01 shows the system's maximum orientation. The ratios in the case of GBFNC are between those for the FC and $BaTiO_3$ (labeled as B). The link between nanofiller concentration and orientation and polymer fibrils may explain this behavior. As a result, the $tan\theta/tan\theta'$ ratio for the undrawn composites $BaTiO_3$ and GBNC is one. Consequently, our findings confirm the rise in orientation with decreasing nanofiller content. The scanning electron microscopy (SEM) on the extruded blends confirms the decrease in their drawing and chain orientation capabilities when the nanofiller content is reduced (to be elaborated later).

2.6.2. Electrical Conductivity

A four-point probe method was used to assess the electrical properties.[58] The average electrical resistance (R) of compression-moulded thin sheets (10 mm × 10 mm × 0.4 mm) was measured using a continuous current source and a voltmeter (Keithley, Ohio, USA). To increase electrical contact in the four-point probe technique, a silver paste was added on the external surface of the composites. All measurements were taken at room temperature, and each composition received an average of five readings.[59,60] The following equations were invoked for the estimation of electrical resistivity and conversion into electrical conductivity, as mentioned in Equations (4) and (5). When t/s is very small ($t << s$), with t being the thickness and s the minimum span between the probes.

$$t\rho = \pi \times t \times \frac{R_{average}}{Ln\,(2)} \tag{4}$$

where $t = 0.4 \times 10^{-1}\ cm$, $s = 2 \times 10^{-1} cm$ and ρ is the voulmetric resistivity. The electrical conductivity (σ) has been estimated by:

$$\sigma = 1/\rho \tag{5}$$

2.6.3. Trans Crystallization Structure by Polarized Light Microscope

A Zeiss polarised light microscope paired with a hot stage arrangement was used to explore the trans-crystallization [58] of polypropylene around in situ fibrils. To avoid the melting of polyethylene terephthalate fibrils during the measurements, the GBFNC-containing fibrils were melted on the sample holder at 180 °C for 5 min to guarantee the homogeneity of the melt. The sample was then cooled at a rate of 10 °C min^{-1} to various crystallization temperatures ranging from 180 to 30 °C. A stepwise chilling regime was used to determine the best conditions for the trans-crystallization of polypropylene around polyethylene terephthalate fibrils. While the sample was cooling, the crystallization was examined with a light microscope.[61]

2.6.4. Differential Scanning Calorimetry

The materials' thermal properties [62] were investigated using DSC (DSC, Q-20, TA Instruments, USA) in nitrogen. The samples were heated from room temperature to 210 °C at a rate of 10 °C min^{-1} and then allowed to cool to room temperature at a rate of 10 °C min^{-1}. The melting and crystallization characteristics of the polypropylene in the nanocomposites were observed. T_c corresponds to the peak crystallization temperature of the polypropylene, Tm is the melting temperature, and H_f is the heat of the fusion of the polypropylene phase in the sample. To

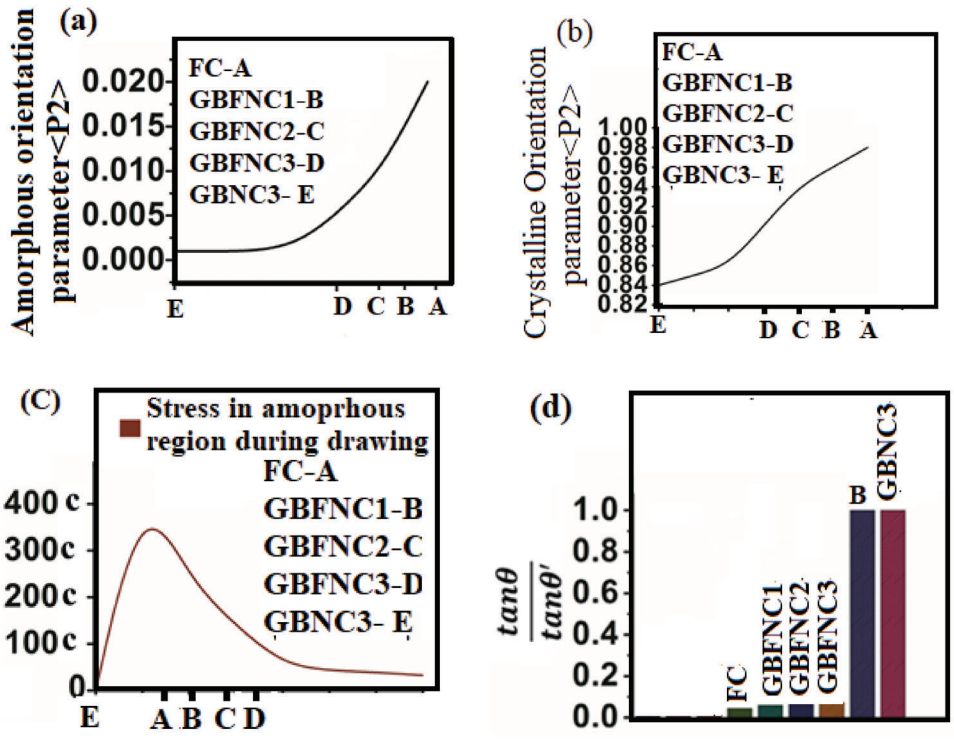

Figure 5. Variation of deformation parameters and fibrils morphology during drawing as a function of nanofillers.

make use of the connection, percentage of the crystallinity of the polypropylene (χ%) was estimated by Equation (6),

$$(\chi\%) = \frac{\Delta H_f \times 100}{\Delta H_{f0}} \times w \tag{6}$$

where ΔH_{f0} is the heat of fusion of 100% crystalline polypropylene, used as 207 J/g, and w is the mass fraction of polypropylene in the blend/composite. Percentage crystallinity is a measurement of the amount of crystalline material in a sample, while degrees of crystallinity (χ_c) is a measurement of the degree of order within the crystalline regions of a material.

2.6.5. Dynamic Mechanical Thermal Analyzer (DMTA)

The examination of viscoelastic properties was conducted with a dynamic mechanical thermal analyzer (DMA 800, Perkin Elmer, USA). Rectangular sample specimens of 12.75 mm × 7.6 mm × 0.5 mm were investigated. The investigation was performed in a single cantilever mode at a recurrence of 1 Hz, from 0 to 150 °C with a heating rate of 2 °C min^{-1}.[63]

2.6.6. Thermal Conductivity by Transient Plane Source (TPS) Method

To determine the thermal conductivity of polymers and polymer nanocomposites, researchers frequently rely on the transient plane source (TPS) technique.[64] This approach involves the use of a compact, thin, and flat sensor that applies a continuous heat flow to the surface of the sample. On the opposite side of the sample, a thermocouple is employed to monitor the temperature increase, allowing for the determination of the sample's thermal conductivity based on the time it takes to reach a steady state. To perform the TPS measurement, a small portion of the sample material is typically crushed into a thin disc or pellet shape with a diameter of ≈10 mm and a thickness of around 0.5 mm. The sample is then placed between the two parts of the TPS sensor, sandwiched in place. Once the sample is secured in the TPS sensor, the system is attached to a computer-controlled data acquisition system. This system provides a steady heat flux to the sample surface and records the temperature rise over time on the opposite side of the sample. Using Equation (7), the thermal conductivity of the sample can be estimated.[64]

$$k = \frac{Q \times t}{\left[4\pi A \left(T_2 - T_1\right)\right]} \tag{7}$$

where k is the thermal conductivity of the sample, Q is the heat flux applied to the sensor, t is the time it takes for the temperature to reach a steady state, A is the area of the sensor, and T_1 and T_2 are the initial and steady-state temperatures recorded by the thermocouple.

2.6.7. Rheological Analysis

Dynamic rheology of polypropylene, B, FC, GBNC1, GBNC2, GBFNC1, GBFNC2 and GBFNC3 was studied using a Modular Rheometer (MCR102, Anton Paar, USA), utilizing a 50 mm parallel plate. Dynamic complex viscosity, storage, and loss moduli

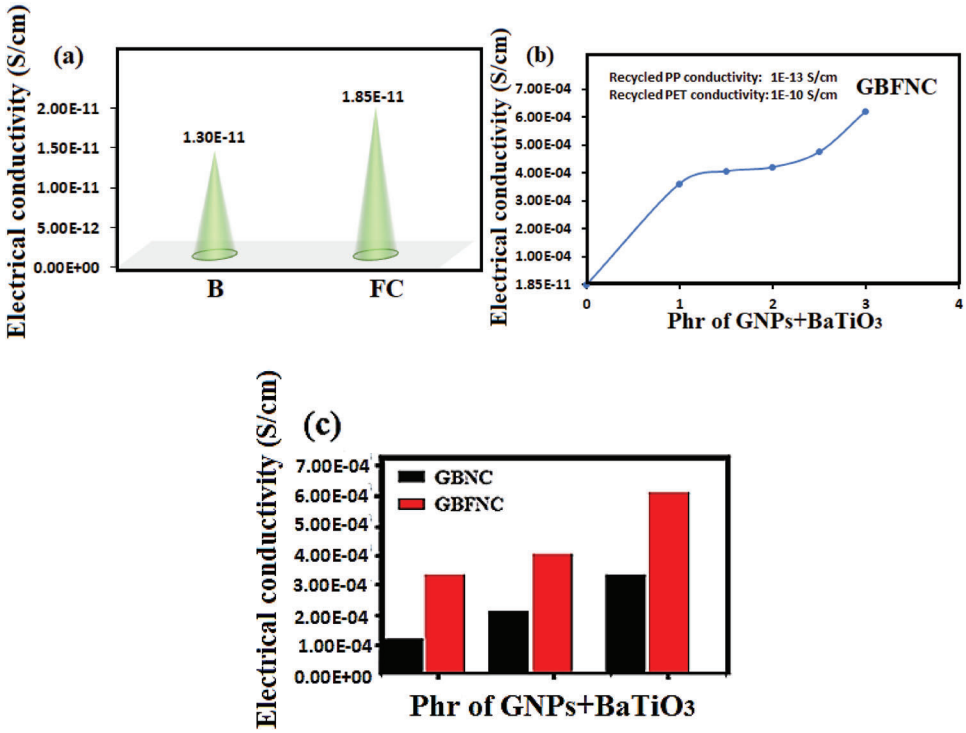

Figure 6. a) Variation of electrical conductivity of PP/PET blend (B) and PP/PET in situ fibrils composites (FC), b) Variation of electrical conductivity of in situ fibrils nanocomposites with varying the phr of GNPs+$BaTiO_3$, c) Variation of electrical conductivity of GNPs+$BaTiO_3$ nanocomposites and in situ fibrils nanocomposites with varying the phr of GNPs+$BaTiO_3$.

were examined as an angular frequency extending from 0.1 to 100 rad s^{-1} at 215 °C and a strain rate of 1% as recommended by.[65]

2.6.8. Static Mechanical Properties

The sample's tensile strength was estimated using a Universal Testing Machine (UTM) (Instron 5900, Instron, USA) at a crosshead speed of 1 mm min^{-1} (as per ASTM standard D882). The load cell had a force of 1000 N and a gauge length of 20 mm.[66]

2.6.9. Atomic Force Microscopy

Atomic force microscopy (AFM) was used extensively for characterizing the surface morphology of samples. An AFM system (Nano Surf Easy Scan2, Switzerland) was used to measure the surface roughness and surface morphology of samples. For the measurement of surface roughness and topology, fracture surfaces were prepared by sample-tearing after their immersion in liquid nitrogen for 2 h.[67]

2.6.10. Morphological Analysis

The morphological investigation was carried out with the aid of a JEOL JSM 6390 scanning electron microscopy. The samples were photographed at a 20 kV acceleration voltage. In the instance of cross-sectional microstructure analysis, fracture surfaces were prepared by cryo-fracturing for 2 h in liquid nitrogen. Prior to SEM, all sample surfaces were coated with a thin layer of gold to make them conductive.[68]

2.6.11. Electromagnetic Interference Shielding by Vector Network Analyzer

EMI shielding is defined as the ability of a material to attenuate an EM signal.[69] It is measured in dB and is the ratio of incident electromagnetic field strength and the transmitted electromagnetic field strength. Here, the effect of morphology and nanofillers on the EMI shielding efficacy has been studied. EMI Shielding effectiveness was measured by using a Vector Network Analyzer (operating at 2.8 GHz) for a sample size of 10 mm × 7 mm × 1 mm.[70]

3. Results and Discussion

3.1. Electrical Conductivity

Figure 6a depicts the DC electrical conductivity values of PP/PET blend (B) and PP/PET in situ fibril composites (FC). Both PP and PET blend(B) and PP/PET in situ fibril composites (FC) are insulating in nature. In this case, the conductivity enhancement due to the inclusion of PET fibers may not be significant, as shown in the figure. However, without additional PET fibrils (e.g., spherical morphology of PET), the electrical conductivity is lower. It is

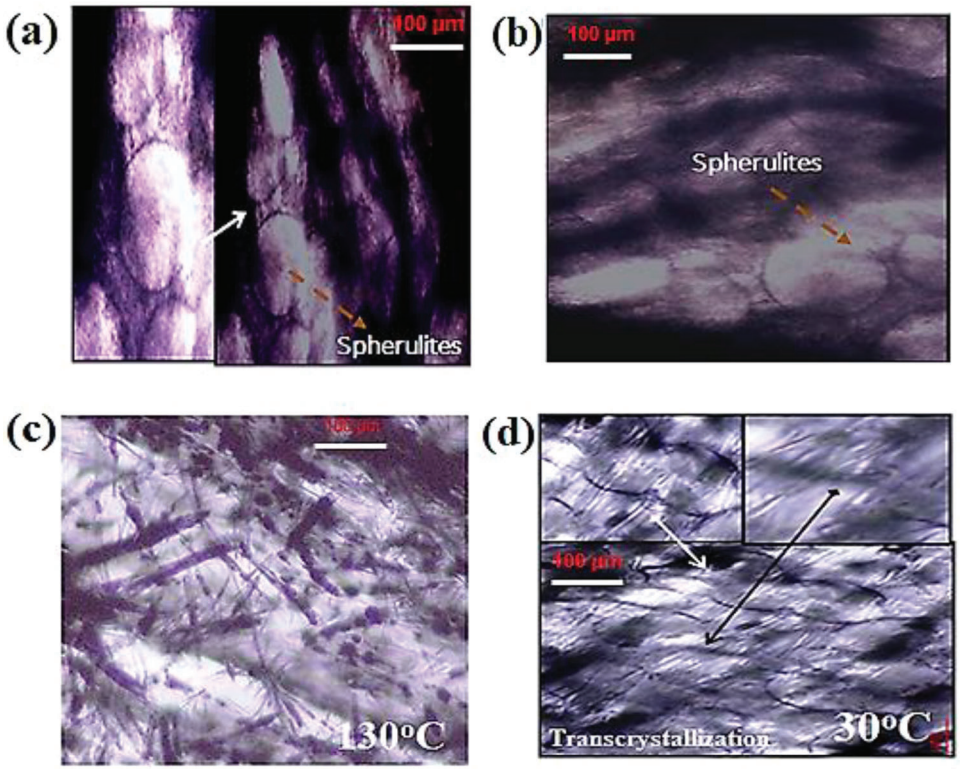

Figure 7. Polarized optical microscopy (POM) microstructure of a) PP/PET Blend (B) at 30 °C as in form of spherulites (Spherical ring), b) PP/PET-GNP-$BaTiO_3$ nanocomposites (GBNC1) at 30 °C as in form of spherulites(Spherical ring), c) PP/PET-GNP- $BaTiO_3$ fibrils nanocomposites (GBFNC1) at 130 °C as in form of transcrystalline growth, d) GBFNC1 at 30 °C as in form of trans-crystalline growth.

observed that the conductivity increases when fibril morphology is introduced into the system.

Figure 6b depicts the DC electrical conductivity values of GBFNC measured by the 4-probe technique and plotted as a function of GNPs+$BaTiO_3$ content (e.g., 1, 2, 3 phr). The conductivity of samples was augmented by increasing the GNPs+$BaTiO_3$ content. A noteworthy improvement in electrical conductivity has been observed with 3 phr of GNPs+$BaTiO_3$ confirming that such composition promotes the development of a significantly increasing electrically conducting network in in situ nanocomposites (GBFNC). Figure 6c shows the DC electrical conductivity for the GBFNC and GBNC. It has been found that the DC conductivity of GBFNC and GBNC is dissimilar for the same content of GNPs+$BaTiO_3$ with GBFNC exhibiting a higher DC conductivity than that of the GBNC, by a minimum order of two. This evidences that nanocomposites of GNPs+$BaTiO_3$ in tandem with in situ fibrils provide a substantially higher electrically conducting network than the GNPs+$BaTiO_3$ based nanocomposites alone. This effect owes to the introduced alignment of the GNPs+$BaTiO_3$ inter-particle separation in the in situ fibrils-based nanocomposites. Therefore, it can be established that the morphology of the polyethylene terephthalate phase also affects the conductivity of nanocomposites. In this research, we found that the morphology of the fibrils plays a significant role in enhancing conductivity. The fibrils exhibit a unique structure that facilitates a tunneling mechanism and creates a current flow path, effectively reducing the spacing distance between fillers. This arrangement leads to a notable enhancement in conductivity. Furthermore, it is important to consider the type of filler used, as it can also impact the conductivity of the fibrils. For instance, carbon black, being a more conductive filler, tends to contribute to higher conductivity compared to graphene platelets. Additionally, the concentration of the filler is another factor influencing the conductivity of the fibrils. Typically, as the concentration of the filler increases, the conductivity of the fibrils shows a corresponding increase. Lastly, the morphology of the system itself can impact the conductivity of the fibrils. For instance, spherical fillers generally exhibit lower conductivity when compared to flake-shaped fillers. These considerations highlight the multifaceted nature of conductivity in fibril-based composites.

3.2. Trans-Crystallization Structure by Polarized Light Microscope

The formation of a transcrystalline layer around the in situ polyethylene terephthalate (PET) fibrils is visualized in **Figure 7**. Figure 7a–d shows the crystal morphology of B, GBNC1, and GBFNC1, where a series of microstructures of the polypropylene (PP) matrix have been formed for different samples at different temperatures. Figure 7a, depicting the crystal morphology of B, shows circular-shaped crystallization patterns, known as spherulites, in a neat PP/PET blend. These spherulites are formed by the crystallization of PP in concentric rings that grow radially. Spherulites are formed by heterogeneous nu-

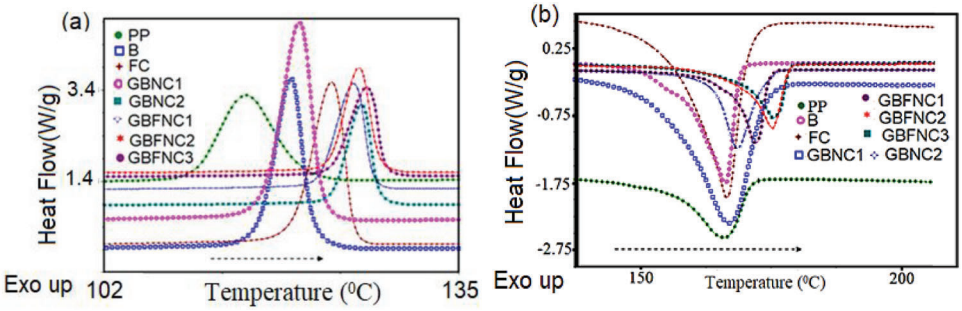

Figure 8. a) Crystallization, b) melting behavior of polypropylene (PP) in B, FC, GBNC1, GBNC2, GBFNC1, GBFNC2, and GBFNC3(Exo up tends to exothermic process).

cleation and favor the increased crystallinity of the PP matrix. Figure 7b shows the crystallization microphotographs of GBNC1 at 30 °C. Compared to the neat PP/PET blend, the spherulites in GBNC1 are smaller in size. In contrast, Figure 7c,d shows the trans-crystallization of the PP matrix in GBFNC1 at different temperatures. This is due to the presence of PET-graphene nanoplatelets-barium titanate (GNPs-$BaTiO_3$) fibrils, which promote the trans-crystalline evolution of PP. In a transcrystalline structure, PP crystals are arranged transversely with respect to the PET-GNPs-$BaTiO_3$ fibril axis (i.e., backbone). The closer proximity of the fibers in GBFNC1 hinders the growth of spherulites at the surface of the PET-GNPs-$BaTiO_3$ fibrils. Overall, the results of this study suggest that the presence of GNPs-$BaTiO_3$ fibrils can promote the trans-crystalline evolution of the PP matrix and lead to smaller spherulites. This has important implications for the design of high-performance polymer composites made by such blends, with improved crystallization behavior, thus improved mechanical properties.

The observed phenomena can be attributed to several factors. First, the incorporation of GNPs-$BaTiO_3$ fibrils into the PP/PET blend provides heterogeneous nucleation sites for PP crystallization. Compared to the neat PP/PET blend, the presence of these fibrils promotes the formation of PP crystals in a trans-crystalline manner rather than the typical spherulitic manner. This trans-crystalline structure offers distinct advantages in terms of mechanical properties and overall performance. Second, the closer proximity of the fibers in the GBFNC1 sample hampers the growth of spherulites on the surface of the PET-GNPs-$BaTiO_3$ fibrils. The fibers act as a physical barrier that impedes the diffusion of PP molecules, which is necessary for the growth of spherulites. As a result, the formation of spherulites is limited, and the crystalline structure becomes more oriented along the fibrils. Lastly, the trans-crystalline structure of the PP matrix in GBFNC1 exhibits enhanced resistance to deformation compared to the spherulitic structure observed in the B and GBNC1 samples. The interconnected nature of the trans-crystalline structure makes it more difficult to break, leading to improved mechanical properties and a higher degree of deformation resistance. Hence, the presence of GNPs-$BaTiO_3$ fibrils in the PP/PET blend promotes trans-crystalline formation, restricts spherulite growth, and enhances the resistance to deformation. These factors contribute to the improved properties observed in the GBFNC1 sample compared to the other samples (B and GBNC1).

3.3. Differential Scanning Calorimetry

Our study included polypropylene (P), an extruded blend of PP/PET (85/15) referred to as B, a composite comprising of a polypropylene matrix and PET fiber (85/15) referred to as FC, and several extruded blend nanocomposites and extruded nanocomposites consisting of a polypropylene matrix, PET fiber, and GNPs-$BaTiO_3$ at different concentrations. We determined the peak crystallization temperature (T_c), melting temperature(T_m), and the heat of fusion(ΔH_f), of the polypropylene phase in the samples using DSC. We also calculated the crystallinity(X_c) of the materials using Equation (6). **Figure 8**a,b depicts the melting and crystallization behavior of polypropylene in the polypropylene-polyethylene-terephthalate blend (B), FC, GBNC1, GBNC2, GBFNC1, GBFNC2, and GBFNC3 groups observed by DCS. The inclusion of polyethylene terephthalate increased the crystallization temperature of polypropylene significantly. The crystallization temperature (T_c) of plain polypropylene was 116 °C, whereas the polypropylene component crystallized at 120 °C in sample B. Because of the existence of long polyethylene terephthalate fibrils functioning as nuclei for polypropylene crystallization, the crystallization temperature of polypropylene was determined to be 124 °C for FC.[71] Along with polyethylene terephthalate fibrils, GNPs-$BaTiO_3$ present in the sample also contributed as nucleating agents in the GBFNC1, GBFNC2 and GBFNC3. Therefore, crystallization of polypropylene shifted toward the higher temperature than those of GBNC1 and GBNC2. The percentage crystallinity (χ%) of the FC is significantly higher than the polypropylene and B, and the percentage crystallinity (χ%) of the GBFNC1, GBFNC2 and GBFNC3 are higher than GBNC1 and GBNC2. The long and slender polyethylene terephthalate (PET) fibrils in FC and PET-GNPs-$BaTiO_3$ fibrils in GBFNC1, GBFNC2, and GBFNC3 act as a region for the trans crystallization of polypropylene. The trans-crystalline layer generated around the fibrils can produce a strong fiber/matrix contact, leading to improved mechanical properties of the resulting nanocomposites. This is because the trans-crystalline structure provides a mechanism for load transfer between the matrix and the reinforcing fibers, which results in an enhanced stiffness and strength. The fascinating observation is that the T_c end set is the highest for GBFNC3. This ascertains that the crystallization process of polypropylene surrounding the polyethylene terephthalate -GNPs-$BaTiO_3$ fibrils in GBFNC1, GBFNC2 and GBFNC3 is prolonged in comparison with B, FC, GBNC1, GBNC2. As

Table 3. Melting, crystallization temperature, percentage crystallinity (χ%), ΔH_f, degrees of crystallinity (X_c), rate constant (k'), and n (Note: T_m(o$_C$),T_c(o$_C$),ΔH_f(J/g),k' (min- ^{1})).

Sample	T_m	T_c	χ%	ΔH_f	X_c	k'	n
Polypropylene	165	116	38	78.66	38.0	0.015	3.3
B	166	120	41	100.1	40.4	0.019	3.1
FC	167	124	44.5	108.3	43.4	0.021	2.9
GBNC1	167.5	121	50.6	122.6	48.2	0.025	3.0
GBNC2	169	125	53.5	129.9	51.3	0.029	–
GBFNC1	172	125.53	55.2	133.9	52.2	0.033	2.6
GBFNC2	175	126	57.4	139.4	54.6	0.037	2.5
GBFNC3	178	127	59.2	78.66	56.5	0.040	3.3

a result, it may be deduced that the morphology and orientation of the dispersed component polyethylene terephthalate-GNPs-$BaTiO_3$ fibrils can tremendously alter the crystallinity of the polypropylene. The values of melting temperature (T_m), crystallization temperature (T_c) and % of crystallinity (χ%) have been tabulated in **Table 3**. Our research has revealed that the T_m and T_c values of materials can vary depending on the composition and concentration of GNPs-$BaTiO_3$. The extruded nanocomposites containing GNPs-$BaTiO_3$ at maximum concentration (GBFNC3) displayed the highest T_m and T_c values, with T_m and T_c values of 178 and 127 °C, respectively. Our findings suggest that adding fibrils and GNPs-$BaTiO_3$ to polypropylene/PET blends and composites can significantly improve crystallinity, with greater effects at higher GNPs-$BaTiO_3$ concentrations. When GNPs-$BaTiO_3$ is introduced to polypropylene-based materials, the percentage crystallinity and heat of fusion increase, as do the melting and crystallization temperatures. This implies that GNPs-$BaTiO_3$ can act as nucleating agents in the materials, promoting crystallization and enhancing the degree of crystallinity. The degree of crystallinity (χ_c) values for various samples are presented in Table 3, which includes Polypropylene, B, FC, GBNC1, GBNC2, GBFNC1, GBFNC2, and GBFNC3. DSC measurements were used to calculate the degree of crystallinity, following the procedure outlined in the previous section. The crystallinity value for polypropylene was found to be 38.0%, while GBFNC3 had a crystallinity value of 56.5%. GBFNC3 showed the highest degree of crystallinity among the samples, while polypropylene exhibited the least. The variations in crystallinity values among the samples can be attributed to differences in molecular structure and processing conditions. These values are valuable for understanding the crystallization behavior of the materials and can be utilized for studying crystallization kinetics. Additionally, this method can provide additional insights into the crystallization process by estimating rate constant k', time of nucleation (t_0), and Avrami exponent or index (n) values for each sample. Overall, our findings suggest that the addition of GNPs-$BaTiO_3$ to polypropylene-based materials can significantly enhance the degree of crystallinity, with the highest crystallinity values observed at higher GNPs-$BaTiO_3$ concentrations. The concentration of GNPs- $BaTiO_3$ and fibrils morphology has two effects on the percentage crystallinity of blend components. First, $BaTiO_3$ acts as a nucleating agent, promoting crystal formation and increasing the crystallinity percentage. Second, $BaTiO_3$ acts as a filler, occupying space in the polymer matrix and hindering crystal growth, also leading to a higher percentage of crystallinity in the blend components. These results offer valuable insights into the properties of nanocomposites and may have implications for the development of new materials with enhanced properties.

The degree of crystallinity, represented by χ_c, is an important parameter for understanding the crystallization behavior of materials. It provides information on the amount of crystallized material at a given time. To determine χ_c, DSC information is collected by heating or cooling the sample at a controlled rate while measuring temperature changes or heat flow. The onset temperature of crystallization is then determined from the DSC curve, which shows a distinct exothermic peak indicating the onset of crystallization. Nonlinear regression analysis is used to fit the curve and obtain values for k', t_0, and n. These values can then be used to calculate the crystallization activation energy. The Avrami equation can be used to approximate the kinetics of the crystallization process based on the DSC data, given by:[62,72]

$$(X_c) = 1 - exp\left[-k'\left(t - t_0\right)^n\right] \tag{8}$$

Using the Avrami equation in MATLAB, one can perform nonlinear regression analysis on experimental data and determine the crystal growth dimension and rate of crystal growth. **Figure 9** displays the n values for various samples, including polypropylene, B, FC, GBNC1, GBNC2, GBFNC1, GBFNC2, and GBFNC3, along with the rate constant data presented in **Figure 10**. The corresponding values of n for each sample are shown in Table 3. The results indicate that n varies across, with polypropylene exhibiting the highest value of 3.3, followed by B with 3.1 and FC with

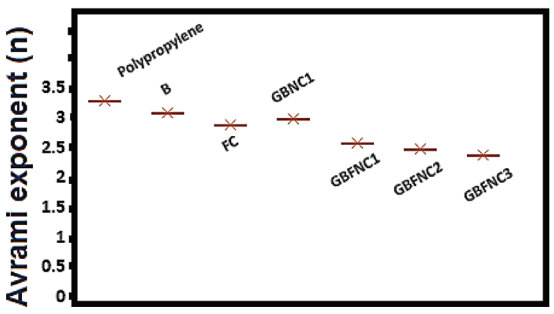

Figure 9. Avrami exponent (n) for polypropylene, B, FC, GBNC1, GBFNC1, GBFNC2, and GBFNC3.

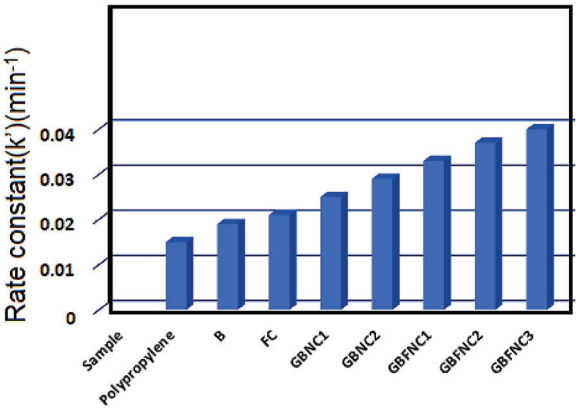

Figure 10. Rate constant (k') for polypropylene, B, FC, GBNC1, GBNC2, GBFNC1, GBFNC2, and GBFNC3.

2.9. The other samples have lower Avrami indices, with GBFNC3 having the lowest value of 2.4. The n is a measure of the type and shape of crystal growth. The value of n smaller than 3 denotes spherulite growth, while a value of 3 indicates lamellar or fibrillar growth. The results reveal that polypropylene, B, and GBNC1 primarily exhibit nodular growth, whereas the other samples display lamellar or fibrous growths. This outcome suggests that the material composition and processing conditions can influence the type and shape of crystal growth. Thus, the crystalline growth of polypropylene, B, and GBNC1 is mainly 3D, whereas GBFNC3 corresponds to more aligned form. This demonstrates the evolution of the transcrystalline structure, as evidenced by the previous section.

The rate constant (k') is a crucial parameter that relates the rate of a chemical reaction to the concentrations of reactants. In the context of crystallization, k' signifies the rate at which a supersaturated solution transforms into a crystalline solid. The higher the temperature, the higher the rate of molecular motion, faster nucleation and crystal growth, and thus higher k' values. k' values for various polypropylene samples range from 0.015 to 0.040 min^{-1}, as shown in Figure 10 and Table 3. The higher the k' value, the faster the material crystallizes. The fastest crystallizing sample, GBFNC3, has a k' value of 0.040 min^{-1}, indicating that a high degree of crystallinity can be reached in a short time. This can be a good candidate for applications that require fast turnaround times. The slowest crystallizing sample, polypropylene, had a k' value of 0.015 min^{-1}, indicating that longer processing times may be required to achieve the desired level of crystallinity. However, polypropylene is still widely used due to its excellent combination of mechanical, thermal, and chemical properties. The k' values of other samples range between 0.019 to 0.040 min^{-1} (Table 3). The addition of GNPs, $BaTiO_3$, and fibrous morphology have a significant effect on increasing the crystallization rate constant (k'), as well as increasing the surface area of the material and providing more sites for nucleation, producing more seed crystals that can grow rapidly into larger crystals. $BaTiO_3$ and fibrils act as effective nucleating agents, promoting crystal nucleation and enhancing the crystal growth rate. Furthermore, GNPs improve the thermal conductivity of the composites, allowing faster heat transfer during crystallization and more efficient cooling, which may also contribute to the overall increase in crystallization.

3.4. Dynamic Mechanical Thermal Analyzer (DMTA)

The storage moduli (E') of polypropylene, B, FC, GBNC1, GBNC2, GBFNC1, GBFNC2 and GBFNC3 are shown in **Figure 11**a. The storage modulus shows the stiffness behavior of the prepared materials. It was observed that the addition of GNPs-$BaTiO_3$ and polyethylene terephthalate fibrils improved the storage modulus of FC, GBNC1, GBNC2, GBNC3, GBFNC1, GBFNC2 and GBFNC3 compared to neat polypropylene and B. The results also describe the effect of the addition of GNPs-$BaTiO_3$ and polyethylene terephthalate (PET) fibrils on the mechanical properties of various composites (FC, GBNC1, GBNC2, GBFNC1, GBFNC2, and GBFNC3) at elevated temperatures. It suggests that the addition of these materials increases the stiffness and elasticity of the composites, and that the fibril morphology of PET has a stronger reinforcing effect than the spherical morphology of PET. The effect of the fibrils is observed at both lower and higher temperatures. However, as the temperature increases above 80 °C, the influence of the fibrils on the storage modulus decreases, causing a decrease in the storage modulus. The decrease in storage modulus observed above 80 °C in the study is likely due to the glass transition temperature (T_g) of PET, which is typically in the range of 70–80 °C. Above this temperature, the PET chains become more mobile, leading to a decrease in the stiffness and reinforcement provided by the fibrils. The storage modulus of GBNC1, GBNC2, GBFNC1, GBFNC2 and GBFNC3 is still greater than polypropylene, B, FC above the 80 °C threshold. The loss modulus (E'') is a measure of the energy dissipated during sinusoidal strain, and it helps to quantify the viscous properties of the sample, as shown in Figure 11b. As the temperature increases, the loss modulus of all the systems studied in the research increases before reaching a maximum and then dropping again. The higher content of GNPs-$BaTiO_3$ and the specific fibril morphology present in the samples lead to a higher loss modulus, indicating a higher energy dissipation and more viscous behavior. This can be attributed to the hindering of the chain mobility of polymer molecules above the glass transition temperature of polypropylene by the GNPs-$BaTiO_3$ and fibrils morphology, which increases energy dissipation due to frictional behavior and increases viscous behavior. The highest loss modulus was observed for GBFNC3, which had the highest content of GNPs-$BaTiO_3$ and the specific fibril morphology. The specific combination of high GNPs-$BaTiO_3$ content and fibril morphology in GBFNC3 resulted in the highest loss modulus, indicating higher energy dissipation at elevated temperatures. This is due to the GNPs-$BaTiO_3$ and fibrils hindering the chain mobility of polypropylene above its glass transition temperature, which increases frictional behavior and energy dissipation at the interface.

To understand the influence of confinement on the mechanical properties of these nanocomposites, the experimental data of Dynamic Mechanical Analysis (DMA) was employed to measure the storage modulus (E') and loss modulus (E'') at different temperatures. The confinement factor was then calculated using the equation: Confinement = (E' – E'') / E'. The confinement of polymer chains on the filler surface is affected by a number of factors, including the type of polymer, the type of filler and reinforcement, the filler and reinforcement content, and the temperature.[73] In general, the confinement of polymer

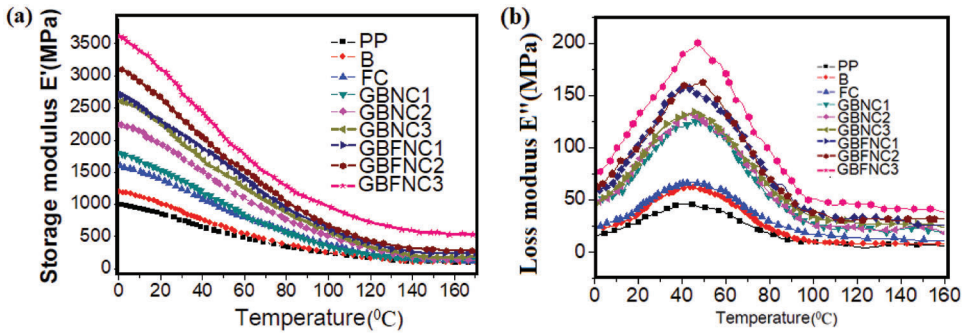

Figure 11. Variation of a) storage modulus, b) Loss modulus of GNPs+$BaTiO_3$ nanocomposites and in situ GNPs+$BaTiO_3$ polyethylene terephthalate (PET) fibrils nanocomposites with varying the phr of GNPs+$BaTiO_3$.

chains increases with increasing the filler and reinforcement content and decreasing temperature.[74] The confinement of polymer chains on the filler surface has a significant impact on the mechanical properties of nanocomposite materials.[75] For example, nanocomposite materials with high confinement of polymer chains typically have higher storage moduli and higher loss moduli.[76] This is because the confined polymer chains are less mobile and more likely to undergo viscous flow.[77] The confinement of polymer chains on the filler surface is also an important factor in the thermal, mechanical, electrical properties of nanocomposite materials. For example, nanocomposite materials with high confinement of polymer chains typically have higher thermal conductivities, higher mechanical and higher dielectric constants. A higher confinement of polymer chains leads to a higher storage modulus and a higher loss modulus.[77] **Table 4** shows the confinement factors of polymer chains on the filler surface in different samples and temperatures. The confinement factors of the polymer chains were determined using dynamic mechanical analysis (DMA). The DMA results showed that the confinement factors of the polymer chains decreased with increasing temperature. This is because the polymer chains become more mobile at higher temperatures, and they are less likely to be confined to the space between the filler particles. The confinement factors of the polymer chains also varied depending on the type of filler. The confinement factors were highest for the nanocomposites that contained GNPs-$BaTiO_3$. This is because GNPs and $BaTiO_3$ have a high surface area, which provides more opportunities for the polymer chains to interact with the filler surface. The results of this study highlight the significant influence of polymer chain confinement on the filler surface in nanocomposites. Understanding and optimizing the confinement of polymer chains can help tailoring the mechanical properties and performance of nanocomposite materials for various applications.

To investigate the reinforcing effect of fillers and fibril shape within the polypropylene matrix, the two-population method was used. This method analyses the mechanical properties of composites with two distinct populations of particles or fibers, each with its own properties, and calculates the overall properties of the composite based on the properties of each population and their concentration.[78] According to this model, the individual reinforcing effects of GNPs-$BaTiO_3$ as well as polyethylene terephthalate fibrils on the elastic performance of the composite can be studied. This additive approach helps determine the reinforcing effect and the morphological effect of GNPs-$BaTiO_3$ within the polypropylene matrix. The effect of GNPs-$BaTiO_3$ was estimated by using the GBNC experiment for conductive ternary blends nanocomposites (CNBC), as mentioned in from Equations (9) to (14), as follows:

$$\frac{E_{GBNC}^{add}}{E_{PP}} = \frac{E_{GNPs-BaTiO3}}{E_{PP}} + \frac{E_{PP/PET(B)}}{E_{PP}} - 1 \tag{9}$$

$$\frac{E_{GBNC}^{add}}{E_{PP}} + 1 = \frac{E_{GNPs-BaTiO3}}{E_{PP}} + \frac{E_{PP/PET(B)}}{E_{PP}} \tag{10}$$

$$E_{GBNC}^{add} + E_{PP} = E_{GNPs-BaTiO3} + E_{PP/PET(B)} \tag{11}$$

Table 4. A comparison table summarizing the confinement of polymer chains on the filler surface for the different samples.

Sample	Confinement Factor at 0 °C	Confinement Factor at 50 °C	Confinement Factor at 90 °C	Significance of Fibrils Morphology and GNPs-BaTiO3
B	0.9792	0.9087	0.9294	–
FC	0.9798	0.9111	0.9333	
GBNC3	0.9815	0.9167	0.9400	The presence of GNPs- $BaTiO_3$ within the polypropylene matrix contributes to the confinement of polymer chains.
GBFNC3	0.9818	0.9280	0.9536	The combination of GNPs- $BaTiO_3$ and polyethylene terephthalate fibrils enhances the confinement of polymer chains on the filler surface.

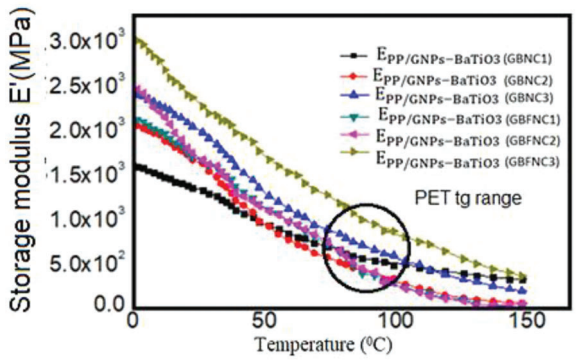

Figure 12. Analysis of storage modulus of GNPs+$BaTiO_3$ nanocomposites and in situ GNPs+$BaTiO_3$ polyethylene terephthalate (PET) fibrils nanocomposites with varying the phr of GNPs+$BaTiO_3$ through two population approach.

$$E^{add}_{GBNC} + E_{PP} - E_{PP/PET(NB)} = E_{PP/GNPs-BaTiO3(GBNC)} \quad (12)$$

For in situ fibrils nanocomposites (GBFNC):

$$\frac{E^{add}_{GBFNC}}{E_{PP}} = \frac{E_{GNPs-BaTiO3}}{E_{PP}} + \frac{E_{FC}}{E_{PP}} - 1 \quad (13)$$

$$E^{add}_{GBFNC} + E_{PP} - E_{FC} = E_{PP/GNPs-BaTiO3(GBFNC)} \quad (14)$$

The reinforcing effect of GNPs-$BaTiO_3$ and polyethylene terephthalate fibrils within the polypropylene matrix was predicted by an additive approach from experimental DMTA data. The additive approach model considered the response of composites constituting an assortment of reinforcing materials within the matrix. In this way, based on the additive approach, this research measured the effect of morphology and concentration of the GNPs-$BaTiO_3$ on the effective storage modulus of the polypropylene matrix. As shown in **Figure 12**, the $E_{PP/GNPs-BaTiO3(GBNC1)}$, $E_{PP/GNPs-BaTiO3(GBNC2)}$, $E_{PP/GNPs-BaTiO3(GBNC3)}$, $E_{PP/GNPs-BaTiO3(GBFNC1)}$, $E_{PP/GNPs-BaTiO3(GBFNC2)}$, $E_{PP/GNPs-BaTiO3(GBFNC3)}$ are the theoretical values obtained by using the model. The theoretical storage modulus value of $E_{PP/GNPs-BaTiO3(GBNC)}$ showed the reinforcement effect of GNPs-$BaTiO_3$ within the polypropylene matrix in the entire temperature range. A coupled influence of GNPs-$BaTiO_3$ and polyethylene terephthalate -GNPs-$BaTiO_3$ fibrils was observed on the storage modulus of polypropylene. It was also found that the GNPs-$BaTiO_3$ had substantial reinforcement effect in the polypropylene matrix at lower as well higher temperatures. The stiffness effect of polyethylene terephthalate-GNPs-$BaTiO_3$ fibrils and GNPs-$BaTiO_3$ was found to be dominant in the case of the polyethylene terephthalate-GNPs-$BaTiO_3$ fibrils, which improved the storage modules. The GNPs-$BaTiO_3$, on account of its high aspect ratio, stiffness, and thermal stability, is a more favorable reinforcing agent at lower and higher temperatures. Furthermore, polyethylene terephthalate fibrils have a positive reinforcing effect along with GNPs-$BaTiO_3$. Henceforth, it could be concluded that polyethylene terephthalate fibrils combined with GNPs-$BaTiO_3$ in situ nanocomposites (GBFNC) can induce a stronger reinforcing effect than merely GNPs-$BaTiO_3$ nanocomposites (GBNC).

3.5. Thermal Conductivity

Figure 13 shows thermal conductivity values for polypropylene, B, FC, GBNC1, GBNC2, GBFNC1, GBFNC2, and GBFNC3. Polypropylene has the lowest thermal conductivity value of 0.218 W m^{-1} K^{-1}, while GBFNC3 has the highest thermal conductivity value of 1.34 W m^{-1} K^{-1} (six times greater), indicating that GBFNC3 transfers heat more efficiently than the other materials. The values are observed varying based on factors such as material composition, microstructure, morphology. For instance, fillers like GNPs and $BaTiO_3$ significantly enhance the thermal conductivity of the polypropylene. The presence of these fillers creates additional heat transfer sites, enhancing heat transfer through the polymer matrix. The morphology of the reinforcement can also affect thermal conductivity, with materials like PET fibrils in GBFNC samples providing high thermal conductivity due to their large surface area and high aspect ratio of graphene nanoplatelets, $BaTiO_3$ and PET fibrils. Similarly, the GNPs and $BaTiO_3$ in the GBNC samples can act as thermal conduits, leading to increased thermal conductivity. Drawing methods such as introducing in situ fibrils and using a drawing-screw extruder unit can improve thermal conductivity via increasing filler dispersion and forming a more uniform fibrils morphology, as seen for the GBFNC samples. Hence, the presence of GNPs and $BaTiO_3$ significantly improves the thermal conductivity of polymers like polypropylene by acting as electrical conduits in the polymer matrix and enhancing heat transfer. In addition, fibrils can further enhance the thermal conductivity. Understanding these factors is crucial in designing materials that meet the required thermal conductivity values for specific applications.

3.6. Rheological Analysis

As shown in **Figure 14**a, the storage modulus (G') values of all samples increased with angular frequency. GBFNC3 has the greatest storage modulus values over the full test frequency range. The inclusion of polyethylene terephthalate fibrils in addition to GNPs-$BaTiO_3$ is the clear cause of GBFNC3's high G'

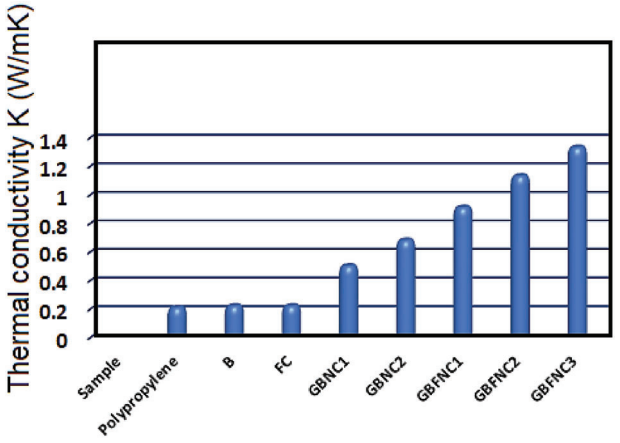

Figure 13. Analysis of Thermal conductivity of GNPs+$BaTiO_3$ nanocomposites (GBNC) and in situ GNPs+$BaTiO_3$ polyethylene terephthalate (PET) fibrils nanocomposites (GBFNC) with varying phr of GNPs+$BaTiO_3$ through two population approach.

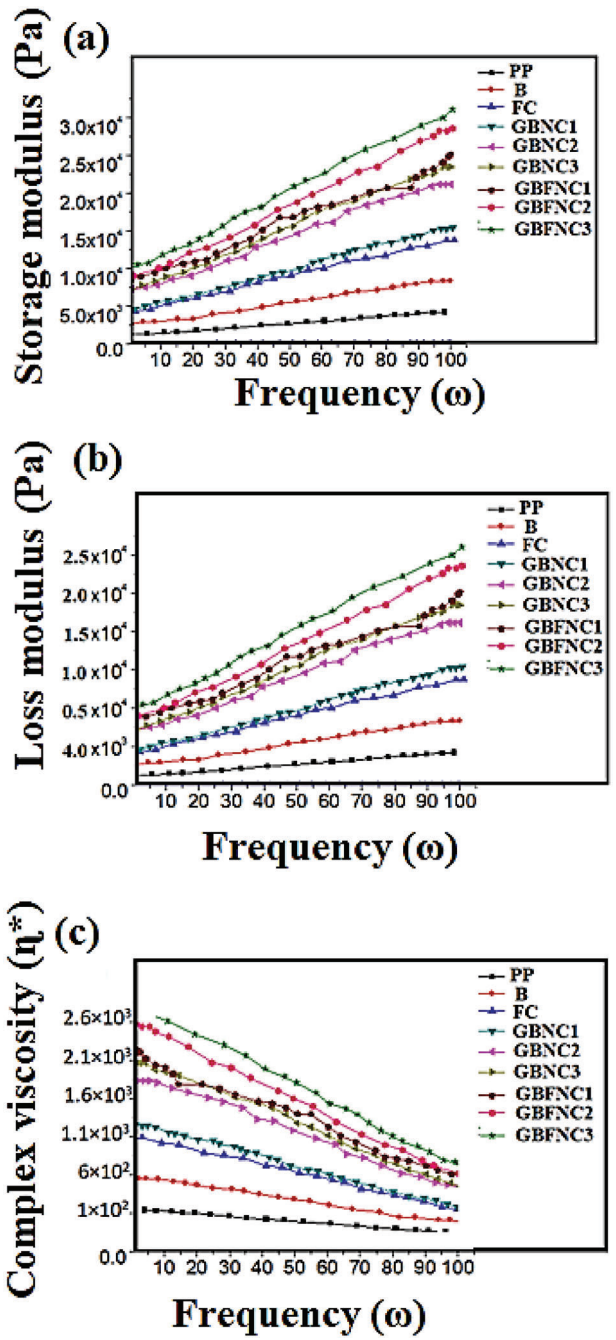

Figure 14. a) Variation of storage modulus with frequency(hertz (Hz)), b) Variation of loss modulus with frequency(hertz (Hz)), c) Variation of complex viscosity with frequency(hertz (Hz)).

values. The storage modulus values of GBNC1, GBNC2, GBFNC1, GBFNC2, and GBFNC3 samples are greater than those of polypropylene, B, and FC. This effect can be attributed to the elastic characteristics of the polypropylene matrix being enhanced by polyethylene terephthalate fibrils and GNPs-$BaTiO_3$. Furthermore, the polypropylene/polyethylene terephthalate blend (B) contains exclusively spherical polyethylene terephthalate domains that are incapable of contributing to the storage modulus like the fibrils in FC, therefore, FC has a higher storage modulus than polypropylene and B. The loss modulus (G'') values were also found to increase with frequency (ω) as shown in Figure 14b. This heralds the viscous behavior of polypropylene, B, FC, GBNC1, GBNC2, GBFNC1, GBFNC2 and GBFNC3. The loss moduli for GBFNC1, GBFNC2 and GBFNC3 were higher than polypropylene, B, FC across the overall frequency range. This indicates that the polyethylene terephthalate fibrils and GNPs-$BaTiO_3$ affect viscous behavior of the composites, however, polyethylene terephthalate fibrils and GNPs-$BaTiO_3$ contribute more to improving the elastic behavior of nanocomposites than the viscous behavior. In comparison to the viscoelastic nature of polypropylene, polyethylene terephthalate inclusions are stiff. Furthermore, the fibrillar shape of the polyethylene terephthalate phase is retained in the isotropic polypropylene matrix, mimicking the environment of fiber-reinforced thermoplastic composites. Figure 14c depicts the complex viscosity (n^*) against angular frequency (ω) curves, where n^* is calculated using Equation (15).

$$n^* = \left[\left(\frac{G'}{\omega}\right)^2 + \left(\frac{G''}{\omega}\right)^2\right]^{1/2} \quad (15)$$

With increasing frequency, the complex viscosity of all samples diminishes (Figure 12c). GBFNC3 has the highest complex viscosity throughout the whole frequency range. The GBNC has a higher n^* than FC, B, and polypropylene. The viscosity of the polypropylene-polyethylene-terephthalate blend is lower than that of FC. This is consistent with the stiffness impact of GNPs-$BaTiO_3$ and polyethylene terephthalate fibrils in the polypropylene matrix at lower and higher frequencies. All the samples, however, show a linear decrease in viscosity with frequency. In contrast to polypropylene, B, and FC, the inclusion of GNPs-$BaTiO_3$ and GNPs-$BaTiO_3$ mixed with polyethylene terephthalate fibrils resulted in a greater reduction of complex viscosity with frequency increase. Moreover, the fibril morphology of the polymer along the GNPs-$BaTiO_3$ leads to shear-thinning behavior at high shear and frequency. This behavior is critical for comprehending how these materials can be used in a variety of applications.

3.7. Mechanical Properties

Tensile testing was used to determine the tensile strength and modulus of the prepared samples, as illustrated in **Figure 15**a,b. The tensile test was performed to assess the amount of reinforcement provided by polyethylene terephthalate fibrils and GNPs-$BaTiO_3$ in the polypropylene matrix. Tensile strength and modulus were measured for polypropylene, B, FC, GBNC1, GBNC2, GBNC3, GBFNC1, GBFNC2, and GBFNC3, and mean tensile strength and modulus values were calculated. Figure 15a shows that the polyethylene terephthalate fibrils morphology in the polypropylene matrix (FC) significantly increases the polypropylene matrix's tension-bearing capacity, which then in turn enhances the tensile strength of FC in comparison to B (spherical microstructures of polyethylene terephthalate). GBFNC3 (fibrils morphology of polyethylene terephthalate-GNPs-$BaTiO_3$) and GBNC3 (spherical structure of polyethylene terephthalate-GNPs-$BaTiO_3$) show a comparable outcome, with GBFNC3 having a

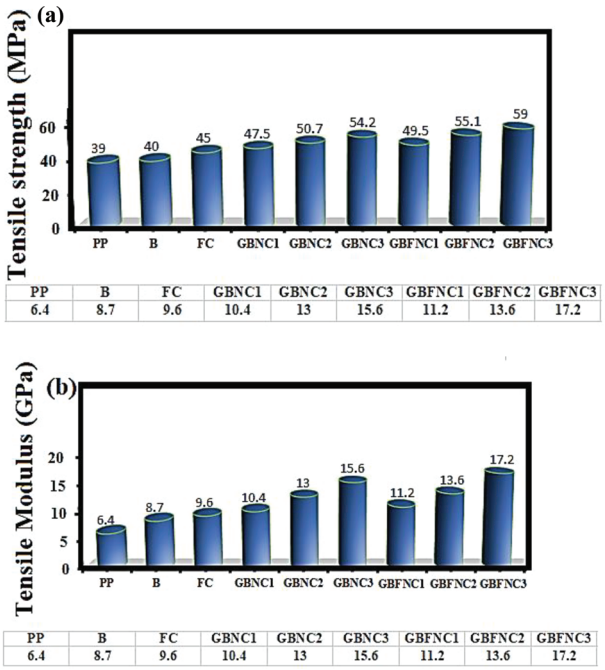

PP	B	FC	GBNC1	GBNC2	GBNC3	GBFNC1	GBFNC2	GBFNC3
6.4	8.7	9.6	10.4	13	15.6	11.2	13.6	17.2

Figure 15. Comparatives study of the a) Tensile strength, b) Tensile modulus of prepared samples.

greater tensile strength than GBNC3. Figure 15a shows that increasing the concentration of GNPs-$BaTiO_3$ in the polypropylene matrix enhanced the system's tensile strength, almost uninterruptedly and coherently. Nevertheless, the combination of polyethylene terephthalate fibrils and GNPs-$BaTiO_3$ improved tensile strength more than simply GNPs-$BaTiO_3$. Two fundamental elements can underlie this: a) polyethylene terephthalate – GNPs-$BaTiO_3$ fibrils work as a superior reinforcing agent and load-bearing component; b) polyethylene terephthalate fibrils with GNPs-$BaTiO_3$ function as a nano-compatibilizer between polyethylene terephthalate fibrils and polypropylene matrix. It demonstrates that GBFNC outperforms polypropylene, B, and GBNC in all situations. Similar patterns were seen for tensile modulus, as illustrated in **Figure 16**b. Figure 16b shows that the polyethylene terephthalate fibrils in the polypropylene matrix (FC) in conjunction with GNPs-$BaTiO_3$ (GBFNC1, GBFNC2 and GBFNC3) significantly increase the tensile modulus of the polypropylene matrix and demonstrate the superiority of GBFNC over other samples in terms of elastic characteristics.

In this section, we delve into the impact of GNPs-$BaTiO_3$ nanoparticles and fibrils morphology on the mechanical properties of PP composites through theoretical calculations. The Halpin-Tsai parameter is a crucial factor in our analysis, as it determines the ratio of the modulus or strength of the constituent material to that of the composite, based on the volume fraction of the constituent material. The analysis focuses on the performance of the composites, determined by the GNPs-$BaTiO_3$ nanoparticles and fiber volume fraction and aspect ratio. We use the reinforcement efficiency factor to measure the effectiveness of the reinforcing fiber in enhancing the properties of the composites. The tensile strength of the matrix material (PP) measures its resistance to deformation under tensile loads, while the tensile strength of the fiber-reinforced material (PET) and GNPs-$BaTiO_3$ nanoparticles measures the strength of the fibers and nanoparticles against deformation under tensile load. It is known that fibrils form a network that directionally reinforces a polymer matrix, thereby improving the composite's mechanical properties. The aspect ratio and surface area of the fibers also impact the mechanical properties of the composite. The increased aspect ratio and surface area of GNPs-$BaTiO_3$ nanoparticles enhance the interfacial adhesion between the fiber and matrix, thereby improving the mechanical properties.

To investigate the mechanical properties of GNPs and $BaTiO_3$ reinforced polypropylene/polyethylene terephthalate, a theoretical calculation was performed using the Halpin-Tsai parameter to determine the reinforcement efficiency factor. It was assumed that the fibers are aligned or likely to be aligned in the direction of mechanical test, therefore would have a strengthening effect in that direction. It was also assumed that GNPs-$BaTiO_3$ is evenly distributed in the blend. The tensile modulus was predicted using the law of mixtures, and the reinforcement efficiency factor was calculated as the ratio between the effective elastic modulus of the composite and the elastic modulus predicted by the mixed law. The aspect ratio of the GNPs/$BaTiO_3$ used in the mixture was ≈296 as calculated below. The material studied in this research included a PP homopolymer, an extruded blend of PP/PET (B) with 85% by weight PP and 15% by weight PET containing PET particles with a diameter of ≈5 microns, and an extruded composite (FC) containing PP/PET fibers with a weight ratio of 85:15 and a PET fiber of 5 microns in diameter and 2 cm in length

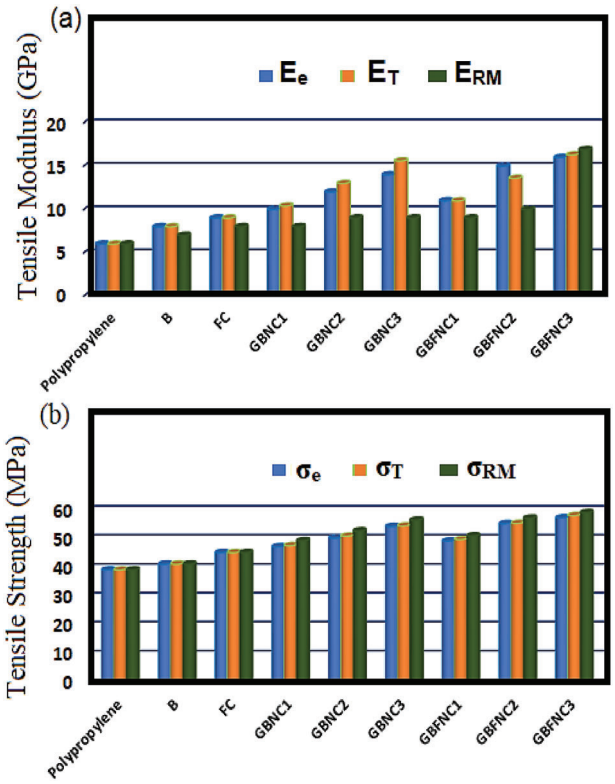

Figure 16. A Comparatives study of the experimental and theoretical for a) tensile moduli and b) strength.

as per our SEM investigations (the 2 cm used as the gauge length during the mechanical testing). The simulations were conducted based on the following assumptions, which are listed below for clarity and precision:

The weight ratio of GNPs to $BaTiO_3$ is considered 1:1, so each constituent have a weight of 0.5 grams. The density range provided for GNPs is 2.0–2.25 g cm^{-3}, so we have used the average density of 2.125 g cm^{-3}. The density of $BaTiO_3$ remained the same at 6.08 g cm^{-3}. The volume of GNPs was calculated as follows: (V_{fGNP}) = 0.5 g / 2.125 g/cm^3 = 0.235 cm^3. The volume of $BaTiO_3$ remained the same: ($V_{fBaTiO3}$) = 0.5 g / 6.08 g/cm^3 = 0.082 cm^3. The volume fraction of GNPs in the mixture was calculated as: (V_{fGNP}) = 0.235 cm^3 / (0.235 cm^3 + 0.082 cm^3) = 0.741. Similarly, the volume fraction of $BaTiO_3$ was calculated as: ($V_{fBaTiO3}$) = 0.082 cm^3 / (0.235 cm^3 + 0.082 cm^3) = 0.259. Using the volume fractions and assuming that the GNPs and $BaTiO_3$ were aligned in the direction of the mechanical testing, and that the aspect ratio of GNPs is 400 and that of $BaTiO_3$ is 1, we have estimated the aspect ratio of the combined GNPs-BaTiO3 as follows:

Aspect Ratio = V_{fGNP} x 400 + $V_{fBaTiO3}$ x 1) / (V_{fGNP} + $V_{fBaTiO3}$) = (0.741×400 + 0.259×1) / (0.741 + 0.259) = 296.26 / 1 = 296.26. The tensile strength of PET fiber is ≈150 MPa. Specimens were tested under unilateral tension. Samples were assumed to be homogeneous and isotropic. The PP/PET (B) granule blend and PP/PET (FC) fiber blend cannot be mixed due to the incompatibility of PP and PET.

The Halpin-Tsai model is commonly used to estimate the composite's basic properties and assumes that fibers are long and thin, with a diameter of approximately [79] 10 micrometers as per the SEM analysis. The volume fraction of fiber is calculated based on the weight fraction of the composite material. Assuming that the Young's modulus of bulk BaTiO3 is ≈75 GPa, while GNP's Young's modulus is ≈1 TPa with an ultimate strength of up to 130 GPa.[64,80,81] Tensile strength and modulus were estimated using the rule of mixtures, which assumes that the composite material behaves as a linear elastic solid. Halpin-Tsai parameter (β) is defined by Equation (16) as a theoretical model to estimate the effective elastic modulus of a composite material. It relates the elastic modulus of a composite to the elastic modulus of the individual constituents and the geometry of the composite structure.[82] The equation was used to calculate the Halpin-Tsai parameter (β) [83]for B, FC, GBFNC, GBFNC nanocomposites consisting of a PPT/PET and GNPS-$BATIO_3$.

$$\beta = \left(\frac{\left(\frac{E_f}{E_m} - 1\right)}{\left(\frac{E_f}{E_m} + f\right)} \right) \tag{16}$$

Here, E_f and E_m are the moduli of elasticity of the reinforcing reinforcement and matrix material, respectively, while f is the reinforcement efficiency factor, which is defined by:

$$f = \left(\frac{\left(1 + \beta\ V_f\right)}{\left(1 -\ V_f \beta\right)} \right) \tag{17}$$

The volume fraction of reinforcement (V_f) is calculated via:

$$V_f = \left(\frac{\left(m_f\right)}{\left(m_f +\ m_m\right)} \right) \times \left(\frac{\left(\rho_m\right)}{\left(\rho_f\right)} \right) \tag{18}$$

where m_f and m_m are the mass fractions of the reinforcement and matrix materials, respectively, and ρ_m and ρ_f are their respective densities. This is applicable for sample B and FC, while the Equation (19) is valid for the other samples such as GBNC and GBFNC.

$$V_f = \left(\frac{\left(m_f\right)}{\left(m_{PET} + m_{BaTiO3} + m_{GNPs} +\ m_m\right)} \right) \times \left(\frac{\left(\rho_m\right)}{\left(\frac{m_{PET} \times \rho_{PET} + m_{BaTiO3} \times \rho_{BaTiO3} + m_{GNPs} \times \rho_{GNPs}}{m_{PET} + m_{BaTiO3} + m_{GNPs}} \right)} \right) \tag{19}$$

where the density of the PET fibrils or density of PET is ρ_{PET} and the densities of the $BaTiO_3$ nanoparticles, GNPs, and PP matrix are ρ_{BaTiO3}, m_{GNPs}, and ρ_m, respectively. m_{PET}, m_{BaTiO3}, and m_{GNPs} are the mass fractions of the PET fiber, $BaTiO_3$ nanoparticles, and GNPs, respectively.

Once above parameters are determined, the theoretical, rule of mixture based tensile strengthh σ_{RM} and modulus E_{RM} can be calculated using the following equations.[84–86] The Halpin-Tsai Equation (20) for theoretical tensile modulus of a composite is:

$$E_{Tc} = E_m \left[\frac{1 + V_f \beta}{1 - V_f \beta} \right] \tag{20}$$

where E_{Tc}= theoretical tensile modulus of the composite E_m = elastic modulus of the matrix material V_f = volume fraction of the reinforcement material β = Halpin-Tsai parameter, which is a measure of the shape and orientation of the reinforcement material in the matrix. The Halpin-Tsai Equation (21) for theoretical tensile strength of a composite is:

$$\sigma_{Tc} = \sigma_m \left[1 + V_f \beta \left(\frac{\sigma_f}{\sigma_m} - 1 \right) \right] \tag{21}$$

where σ_{Tc}= theoretical tensile strength of the composite and σ_m = tensile strength of the matrix material. Finally, the tensile strength σ_{RM} and tensile modulus E_{RM} of blend, composites, nanocomposites are given by:

$$\sigma_{Tc} = \left(1 - V_f\right) \sigma_m + V_f \sigma_f \tag{22}$$

$$E_{RM} = \left(1 - V_f\right) E_m + V_f E_f \tag{23}$$

where σ_m and E_m are the tensile strength and modulus of the matrix material, while σ_f and E_f are those of the reinforcing fibers. **Table 5** presents the analysis of various composite materials based on PET fibers and PET fibers reinforced with GNP-$BaTiO_3$ particles. The composites were analyzed for their mechanical properties, including modulus and strength. The table also includes the percentage of PET and GNP-$BaTiO_3$ by weight and volume, respectively, for each sample. Theoretical tensile

Table 5. Comparison of Theoretical mechanical properties for PP/PET blends with different reinforcement types and concentrations.

Sample	PET wt.%	GNPs-BaTiO3 vol%	Halpin-Tsai Parameter	Rule of Mixtures Predicted Modulus (GPa)	Theoretical Tensile Modulus (GPa) Halpin-Tsai	Theoretical Tensile Strength (MPa) Halpin-Tsai	Rule of Mixtures Tensile Strength (MPa)	Reinforcement Efficiency
PP	0	0	–	6	6	39	39	–
B	15	0	0.0215 (w.r.t PET)	8	7	41	41	0.17 (w.r.t PET)
FC	15	0	0.027 (w.r.t PET)	9	8	45	45	0.224 (w.r.t PET)
GBNC1	15	0.22 (1phr)	0.181	10.4	8	47.4	49.1	0.324
GBNC2	15	0.44 (2phr)	0.251	13.0	9	50.7	52.5	0.468
GBNC3	15	0.66 (3phr)	0.317	15.6	9	54.2	56.2	0.534
GBFNC1	15	0.22 (1phr)	0.181	11.0	9	49.5	50.8	0.324
GBFNC2	15	0.44 (2phr)	0.251	13.6	10	55.1	56.9	0.468

modulus and strength are calculated based on the properties of the individual constituents by Halpin-Tsai parameter model, whereas the rule of mixture predicts the modulus and strength for the composites. Reinforcement efficiency factor is defined as the ratio of experimental modulus or strength to the theoretical values predicted by the Rule of Mixtures. This suggests that the PET fibrils are effectively reinforcing the PP matrix, resulting in an improvement in mechanical properties. The reinforcement efficiency factor also provides insight into the effectiveness of the reinforcement. As seen in the table, the efficiency factor increases with increasing GNP-$BaTiO_3$ volume fraction, indicating that the particles are effectively reinforcing the PP matrix.

Figure 16 presents the results of an experiment that was conducted to measure the tensile strength and modulus of various composite materials, including PP, B, FC, GBNC1, GBNC2, GBNC3, GBFNC1, GBFNC2, and GBFNC3. Figure 16 shows the experimental tensile moduli and strength for the different materials (blue bars), along with their corresponding theoretical moduli predicted above from the Halpin-Tsai equation (green bar) and the rule of mixture (orange bar), demonstrating an accurate prediction for the tensile strength (and not the moduli) by the theory. The moduli for the GBFNC3 was accurately predicted by the theory.

3.8. Atomic Force Microscopy

Surface morphology plays a critical role in determining the physical and chemical properties of materials, was investigated using Atomic Force Microscopy (AFM) and results are shown in **Figure 17**a–f. The AFM images provided valuable insights into the distinct morphologies exhibited by each sample.

The AFM images provided clear visual representations of the surface morphology for each sample. Figure 17a displayed the surface morphology of PP. In Figure 17b, the blend B showed spherical distributions of polyethylene terephthalate within the polypropylene matrix. Figure 17c exhibited the fibrillar morphology of the polypropylene/polyethylene terephthalate in situ fibrils composites FC, indicating the presence of elongated structures within the composite. The distribution of GNPs/$BaTiO_3$ within the polypropylene matrix for the GBNC1 sample is displayed in Figure 17d, while Figure 17e,f demonstrated the distribution of GNPs/$BaTiO_3$ and the fibrillar morphology for the nanocomposites GBFNC with 1 and 3 phr of GNPs-$BaTiO_3$, respectively.

The AFM images presented distinct surface morphologies for each material. The spherical distribution of polyethylene terephthalate within the polypropylene matrix in the polypropylene-polyethylene-terephthalate blend in sample B suggests phase separation and could have implications for the material's mechanical and thermal properties. The presence of fibrillar structures in the polypropylene/polyethylene terephthalate in situ fibrils composites in sample FC indicates enhanced interfacial adhesion and the potential for improved mechanical performance. The distribution of GNPs/$BaTiO_3$ within the polypropylene matrix for the GBNC1 sample suggests effective dispersion, which could lead to enhanced electrical and thermal properties. The presence of GNPs/$BaTiO_3$ in the polypropylene/polyethylene terephthalate-GNPs/$BaTiO_3$ in situ fibrils in samples GBFNC further modifies the morphology, potentially resulting in improved multifunctional properties. To verify the surface morphology observations seen in the AFM study, we referred to previous research papers that reported relevant results. Specifically, we examined the findings from a study that presented AFM images of untreated PET samples, showcasing the surface morphology of graphene nanoplates obtained through exfoliation using potassium. These images helped support our understanding of the spherical distribution of polyethylene terephthalate within the polypropylene matrix observed in sample B.[87,88] Additionally, we referred to another study that provided AFM images of $BaTiO_3$ thin films, both untreated and irradiated at a dosage of 1×10^{11} ions cm^{-2}. These images aided in understanding the distribution of GNPs- $BaTiO_3$ within the polypropylene matrix in the GBNC1 sample, which demonstrated effective dispersion of the nanoparticles.[89] Furthermore, we considered the findings of a separate study that revealed elementary fibrils on the surfaces of parenchyma-type secondary walls (pSW).[90] This information supported our interpretation of the fibrillar morphology observed in sample FC and in the nanocomposites samples, GBFNC, with 1 and 3 phr of GNPs-BaTiO3. By incorporating these references, we have enhanced the scientific validity and credibility of our analysis of the surface morphology observed in the investigated materials. In conclusion, AFM was successfully utilized to investigate the surface morphology of our samples, revealing distinctive morphologies

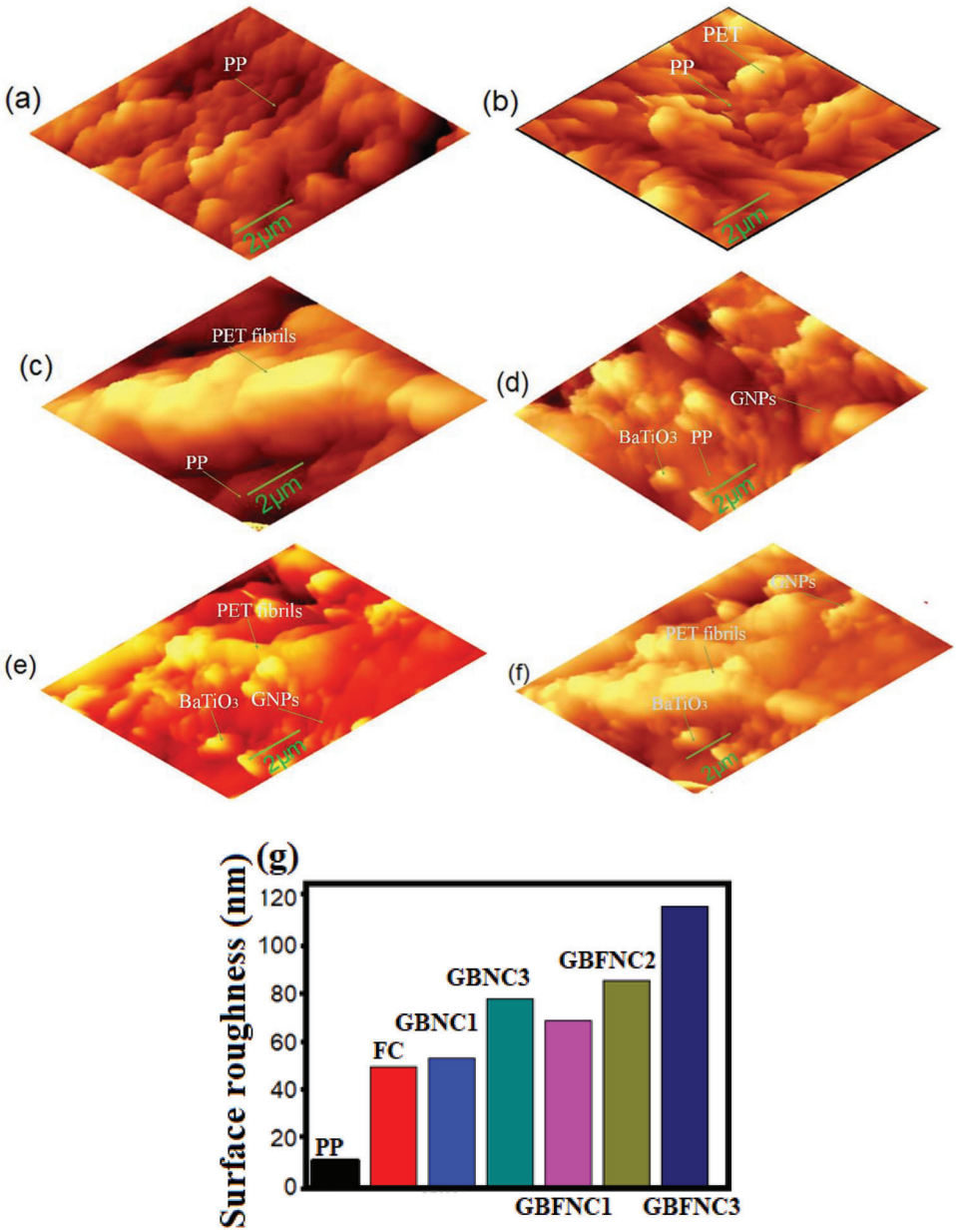

Figure 17. AFM images and surface roughness of samples, a) Polypropylene (PP), b) Polypropylene (PP)/ polyethylene terephthalate (PET) blend (B), c) Polypropylene (PP)/ polyethylene terephthalate (PET) in situ fibrils composites (FC), d) GBNC1, e) GBFNC1, f) GBNFC3, g) Surface roughness.

for each material, offering valuable insights into their surface characteristics. Further investigation and analysis are necessary to elucidate the relationship between these morphological features and the material's properties, enabling the development of advanced functional materials with tailored performance.

Surface roughness is an essential parameter influencing the functional properties of materials. This study investigates the influence of morphology and GNPs- $BaTiO_3$ content on the surface roughness of polypropylene-based nanocomposites. The surface roughness was characterized using Atomic Force Microscopy (AFM), and the relationship between morphology, GNPs- $BaTiO_3$ content, and surface roughness was analyzed. AFM was employed to assess the surface roughness of the investigated materials. Images were captured for polypropylene (PP), polypropylene-polyethylene-terephthalate blend (B), polypropylene/polyethylene terephthalate in situ fibrils composites (FC), GNPs- $BaTiO_3$ within the polypropylene matrix (GBNC1), and polypropylene/polyethylene terephthalate-GNPs- $BaTiO_3$ in situ fibrils nanocomposites (GBFNC) with varying GNPs- $BaTiO_3$ content. The obtained AFM images were analyzed to quantify and compare the surface roughness of each sample. Figure 17g presents the AFM image demonstrating the surface roughness of polypropylene, B, FC, GBNC1, GBFNC1, GBFNC2, and GBFNC3. It is observed that the surface roughness is influenced

by both the morphology of the samples and the GNPs- $BaTiO_3$ content. The presence of fibrils morphology in FC and GBFNC samples significantly increased the surface roughness, indicating the development of textured structures on the material's surface. Moreover, an increase in the GNPs- $BaTiO_3$ content also contributed to higher surface roughness. Furthermore, the combination of GNPs- $BaTiO_3$ and polyethylene terephthalate fibrils exhibited a pronounced effect on the surface roughness of the samples. Notably, GBFNC3, with the highest GNPs- $BaTiO_3$ content, demonstrated the highest surface roughness among all the investigated samples. The observed inccrease in surface roughness can be attributed to several factors. The presence of fibrils morphology introduces additional roughness features on the material's surface, resulting in enhanced roughness values. Additionally, the higher content of GNPs- $BaTiO_3$ promotes agglomeration or dispersion of nanoparticles, thereby further modifying the surface morphology and increasing the surface roughness. The combination of GNPs-BaTiO3 with polyethylene terephthalate fibrils creates a pronounced impact on the surface roughness. The interaction between these components influences the formation of surface features, resulting in higher roughness values.

3.9. Morphological Analysis

In **Figure 18**a–g, SEM microstructures of various materials are presented, including polypropylene (PP), polypropylene-polyethylene-terephthalate blend (B), in situ fibrils microfibrillar composites (FC), GNPs-BaTiO3-based nanocomposites with different concentrations (GBNC1 and GBNC3), and GNPs-BaTiO3-based in situ fibrils nanocomposites with different concentrations (GBFNC1 and GBFNC3). Figure 18a displays the morphology of neat PP, while Figure 18b illustrates the unique morphology of the polypropylene-polyethylene-terephthalate blend (B). B's morphology results from coalescence and breakup of polyethylene terephthalate particles during extrusion, leading to their distribution as spherical and curved shapes within the polypropylene matrix. Elongation forces during extrusion are evident from the curved morphology of the polyethylene terephthalate component, causing its distribution as beads in polypropylene. Figure 18c confirms the generation of in situ polyethylene terephthalate fibrils throughout the drawing process, with their diameters falling within the micrometer range. This indicates the formation of fibrillar structures in the composites, significantly influencing their mechanical properties. Figure 18d,e depict the morphology of GNPs-BaTiO3-based nanocomposites (GBNC1 and GBNC3). Here, the absence of fibrils morphology and the uniform distribution of GNPs-BaTiO3 particles can be noticed. GNPs-BaTiO3 nanoparticles influence the polymer matrix's crystallization behavior and lead to a uniform dispersion within it.

To gain a deeper understanding of the morphological differences, images of GBNC (GBNC1 with 1 phr of GNPs-BaTiO3 and GBNC3 with 3 phr of GNPs-BaTiO3) were compared with those of GBFNC (GBFNC1 with in situ polyethylene terephthalate fibrils along with 1 phr of GNPs-BaTiO3 and GBFNC3 with in situ polyethylene terephthalate fibrils with 3 phr of GNPs-BaTiO3). Figure 18f,g represent the morphology of GBFNC1 and GBFNC3, respectively, where GNPs-BaTiO3 nanoparticles are

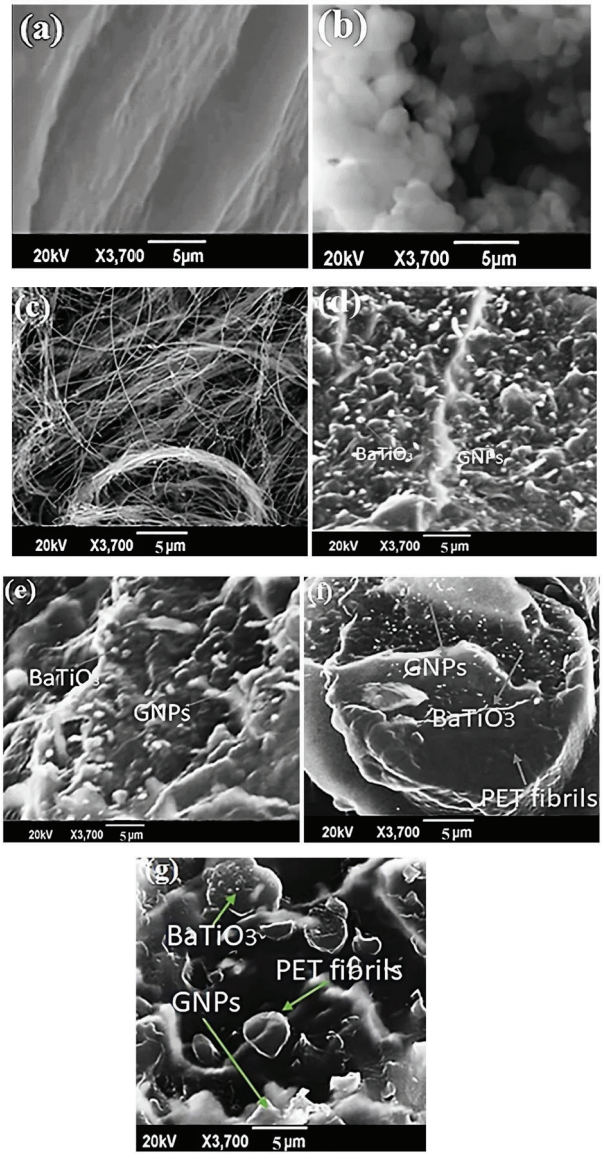

Figure 18. SEM images, a) Polypropylene (PP); b) Polypropylene (PP)/ polyethylene terephthalate (PET) blend after surface extraction of polypropylene (PP) by hot xylene (B); c) polypropylene (PP)/ polyethylene terephthalate (PET) in situ fibrils composites after surface extraction of polypropylene by hot xylene (FC), d) GBNC1 cryo- fractured surfaces, e) GBNC3 cryo-fractured surfaces, f) GBFNC1 cryo- fractured surfaces, g) GBNFC3 cryo-fractured surfaces.

combined with in situ fibrils, and the fibrils' diameters remain in the micrometer range. Interestingly, the diameters of the fibrils in GBFNC1 and GBFNC3 are larger than those observed in neat in situ polyethylene terephthalate fibrils, in line with previous theoretical calculations.

The SEM images of GNPs-BaTiO3 nanoparticles typically reveal their distinctive 2D structure. GNPs, or graphene nanoplatelets, are characterized by thin and flat nanoplatelets with a highly ordered arrangement of carbon atoms. This unique structure gives them excellent mechanical, electrical, and

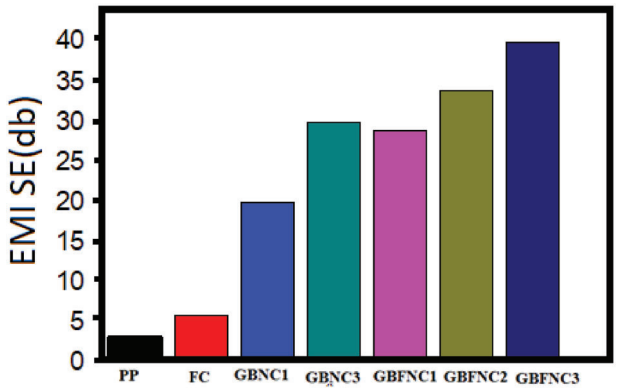

Figure 19. Electromagnetic shielding effectiveness of polypropylene (PP), FC, GBNC1, GBNC3, GBFNC1, GBFNC1, GBFNC3.

thermal properties, making them desirable reinforcements in nanocomposites. On the other hand, SEM images of in situ fibrils showcase the morphology of the polyethylene terephthalate (PET) fibrils that have been generated throughout the drawing process. These fibrils have diameters within the micrometer range. The formation of fibrillar structures in composites significantly influences their mechanical properties, contributing to enhanced strength and stiffness.[45,91] When combined in nanocomposites, such as GNPs-BaTiO3-based in situ fibrils nanocomposites (GBFNC), SEM images depict the coexistence of both GNPs-BaTiO3 nanoparticles and in situ fibrils.[92] The presence of GNPs-BaTiO3 nanoparticles restricts the orientation of the polymer chains and bears the elongational force, reinforcing the composites and leading to increased stiffness. In summary, SEM microstructures offer valuable insights into the morphology of different composites, and the presence of GNPs-BaTiO3 nanoparticles and in situ fibrils significantly influence their properties and mechanical performance. The combination of different materials and their morphologies plays a crucial role in tailoring the mechanical characteristics of the composites for specific applications in diverse fields.

3.10. Electromagnetic Interference Shielding by Vector Network Analyzer

Figure 19 illustrates the influence of morphology and GNPs-$BaTiO_3$ concentration on the shielding effectiveness (SE) of polypropylene-based blends and nanocomposites against electromagnetic interference (EMI). EMI poses significant challenges in various industries as it leads to signal interference, data corruption, and equipment failure. Materials with high electrical conductivity and dielectric constant are utilized as EMI shielding materials to address this issue. The aim of this research was to investigate the impact of morphology and GNPs-$BaTiO_3$ concentration on the SE of polypropylene-based blends and nanocomposites. The materials were prepared through melt blending, and the SE was evaluated using a standard EMI shielding test. The results demonstrated a clear relationship between the GNPs- $BaTiO_3$ content and the SE. Increasing the concentration of GNPs- $BaTiO_3$ improved the SE of the materials. This enhancement can be attributed to the conductive and dielectric nature of GNPs- $BaTiO_3$ particles, which create pathways for the reflection, absorption, and dissipation of electromagnetic waves. Additionally, the morphology of the materials significantly influenced their SE. Among the investigated samples, the material with in situ polyethylene terephthalate (PET) fibrils exhibited the highest SE. This outcome can be attributed to the larger surface area provided by the fibrils, facilitating enhanced interaction with the GNPs- $BaTiO_3$ particles and further improving the SE of the material. $BaTiO_3$ acts as a dielectric filler within the polymer matrix, providing pathways for electromagnetic wave absorption and dissipation. GNPs, serving as conductive fillers, improve the electrical conductivity of the material, facilitating the attenuation of electromagnetic waves and enhancing the EMI shielding properties. PET fibrils, with their high aspect ratio and increased surface area, play a crucial role in enhancing EMI shielding capabilities. These fibrils enhance the interaction between conductive fillers and the polymer matrix, resulting in improved electrical conductivity and EMI shielding performance. The combination of $BaTiO_3$ and GNPs within the polymer matrix exhibits a synergistic effect on EMI shielding properties, surpassing the individual shielding effectiveness of $BaTiO_3$ or GNPs alone. Material morphology significantly influences EMI shielding properties. The presence of PET fibrils increases the material's surface area, facilitating enhanced interaction between the conductive fillers and the polymer matrix, and contributing to improved electrical conductivity and overall EMI shielding performance. Materials incorporating BaTiO3, GNPs, and PET fibrils exhibit enhanced EMI shielding properties, making them suitable for various applications, including electronic devices, automotive systems, aerospace equipment, and other industries where reliable EMI protection is essential. This study highlights the potential for enhancing the SE of polypropylene-based blends and nanocomposites by increasing the GNPs- $BaTiO_3$ concentration and manipulating the material's morphology. These findings have important implications for the development of novel EMI shielding materials suitable for a wide range of applications. By understanding the relationship between morphology, GNPs- $BaTiO_3$ concentration, and SE, researchers and engineers can design and optimize EMI shielding materials to meet specific requirements. The ability to tailor the SE of materials opens up opportunities for applications in industries such as electronics, telecommunications, aerospace, and automotive, where effective EMI protection is crucial. The impact of BaTiO3, GNPs, and PET fibrils on EMI shielding is substantial. $BaTiO_3$ acts as a dielectric filler, while GNPs provide conductivity, and PET fibrils enhance material surface area, resulting in improved electrical conductivity and enhanced EMI shielding capabilities. Understanding the synergistic effects and morphology-related enhancements enables the development of advanced EMI shielding materials tailored to specific application requirements. These findings contribute to the advancement of EMI shielding technologies, promoting improved performance and reliability in the face of increasing EMI challenges.

4. Conclusions

This article presents a detailed study on a scalable process to produce nanocomposite fibrils made from PP/ PET combined with high-aspect-ratio functional materials (GNPs/BaTiO3) leading to a process development that can remanufacture

high-performance, multifunctional composites. The nanocomposites examined in the current research showed unprecedented electrical conductivity, thermomechanical properties and electromagnetic interference shielding. The research demonstrated that recycled and functionalized material systems can be reliably remanufactured with an ultimate aim of minimal waste and emissions, offering potential for various sustainable applications in electronics, energy storage, biomedical and transport sectors. Moreover, the orientation parameters and fibril morphology of the functional polymer systems were observed to be significantly affected by nanofiller concentration, with effects on stiffness, viscosity, and deformation behavior, offering tunable properties. The electrical conductivity x in situ fibrils with 3 phr of GNP-$BaTiO_3$ (GBFNC3) was improved due to enhancement in its conductive network formation and reduced inter-particle separation, influenced by PET phase morphology. Optimal trans-crystallization of PP around in situ PET-GNPs-$BaTiO_3$ fibrils was achieved using a stepwise cooling regime, promoting transcrystalline evolution, and altering spherulite growth. The presence of PET and PET-GNPs-$BaTiO_3$ fibrils in nanocomposites significantly affects PP crystallization, thus enhancing crystallinity and altering thermal properties. GNPs/$BaTiO_3$ and PET fibrils enhanced storage modulus and stiffness in PP matrix, with GNPs/$BaTiO_3$ providing reliable reinforcement at various temperatures and PET fibrils being effective below 80 °C. Rheological analysis revealed that incorporating PET fibrils and GNPs-$BaTiO_3$ improved elastic properties and viscous behavior in PP matrix, with GBFNC3 exhibiting highest storage modulus and complex viscosity. The tensile strength and modulus were also improved with the PET fibrils and GNPs-$BaTiO_3$ in the PP matrix, thus enhancing mechanical properties and surface roughness. It was extensively observed that the fibril morphology and higher GNPs-$BaTiO_3$ content contributed significantly to such properties. Furthermore, increased GNPs-$BaTiO_3$ content and the presence of in situ PET fibrils improved EMI shielding effectiveness, confirming the reinforcing effect and enhanced attenuation of EM waves with possible exploitation for scalability of such remanufactured multifunctional nanocomposites.

Acknowledgements

The research received funding from the Engineering & Physical Sciences Research Council (EPSRC), UK – Ref. EP/R016828/1 (Self-tuning Fibre-Reinforced Polymer Adaptive Nanocomposite, STRAIN comp) and EP/R513027/1 (Study of Microstructure of Dielectric Polymer Nanocomposites subjected to Electromagnetic Field for Development of Self-toughening Lightweight Composites).

Conflict of Interest

The authors declare no conflict of interest.

Data Availability Statement

The data that support the findings of this study are openly available in City, University of London at https://doi.org/10.25383/city.22339807, reference number 22339807.

Keywords

barium titanate, electromagnetic interference shielding, graphene nanoplatelets, multifunctional composites, nanocomposite fibrils, thermal stability

Received: May 3, 2023
Revised: July 29, 2023
Published online:

[1] J. R. Jambeck, R. Geyer, C. Wilcox, T. R. Siegler, M. Perryman, A. Andrady, R. Narayan, K. L. Law, *Science* **2015**, *347*, 768.
[2] S. Lotfian, C. Giraudmaillet, A. Yoosefinejad, V. K. Thakur, H. Y. Nezhad, *ACS Omega* **2018**, *3*, 8891.
[3] E. Naderi Kalali, S. Lotfian, M. Entezar Shabestari, S. Khayatzadeh, C. Zhao, H. Yazdani Nezhad, *Curr. Opin. Green Sustain. Chem.* **2023**, *40*, 100763.
[4] D. An, S. Lotfian, D. Mesbah, D. Ayre, A. Yoosefinejad, V. K. Thakur, H. Yazdani Nezhad, *Mater. Today Chem.* **2019**, *14*, 100202.
[5] R. Mudhar, A. Mucolli, J. Ford, C. Lira, H. Yazdani Nezhad, *J. Compos. Sci.* **2022**, *6*, 345.
[6] S. Hawi, S. Gharavian, M. Burda, S. Goel, S. Lotfian, T. Khaleque, H. Y. Nezhad, *Emergent Mater.* **2021**, *4*, 1679.
[7] B. E. Bagui, L. R. A. C. Arellano, *Int. J. Qual. Res.* **2021**, *1*, 150.
[8] D. Li, J. Barrington, S. James, D. Ayre, M. Sloma, M.-F. Lin, H. Yazdani Nezhad, *Sci. Rep.* **2022**, *12*, 7504.
[9] T. L. Dora, A. Owhal, T. Roy, S. U. Belgamwar, S. Goel, H. Y. Nezhad, R. R. Mishra, *Mater. Today Commun.* **2023**, *35*, 105693.
[10] R. Kumar Mishra, S. Goel, H. Yazdani Nezhad, *Biomater. Polym. Horizon* **2021**, *1*, 1.
[11] T. Bregar, D. An, S. Gharavian, M. Burda, I. Durazo-Cardenas, V. K. Thakur, D. Ayre, M. Sloma, M. Hardiman, C. Mccarthy, H. Yazdani Nezhad, *Sci. Rep.* **2020**, *10*, 16833.
[12] S. Rout, R. K. Nayak, S. C. Patnaik, H. Yazdani Nezhad, *J. Compos. Sci.* **2022**, *6*, 245.
[13] M. S. Jayalakshmy, R. K. Mishra, in *Carbon-Based Nanofillers and Their Rubber Nanocomposites : Fundamentals and Applications*, Elsevier, New York, **2019**, Ch 14.
[14] R. K. Mishra, S. Loganathan, *Mod. Chem Appl.* **2017**, *5*, 1.
[15] R. K. Mishra, J. Abraham, K. Joseph, K. Jayanarayanan, N. Kalarikkal, S. Thomas, in *Polyurethane Polymers: Composites and Nanocomposites*, Elsevier, New York, **2017**, Ch. 12.
[16] R. K. Mishra, J. Abraham, N. Kalarikkal, K. Jayanarayanan, K. Joseph, S. Thomas in *Polyurethane Polymers: Blends and Interpenetrating Polymer Networks*, Elsevier, New York, **2017**, Ch. 8
[17] A. H. Alias, M. N. Norizan, F. A. Sabaruddin, M. R. M. Asyraf, M. N. F. Norrrahim, A. R. Ilyas, A. M. Kuzmin, M. Rayung, S. S. Shazleen, A. Nazrin, S. F. K. Sherwani, M. M. Harussani, M. S. N. Atikah, M. R. Ishak, S. M. Sapuan, A. Khalina, *Coatings* **2021**, *11*, 1355.
[18] Z. Han, A. Fina, *Prog. Polym. Sci.* **2011**, *36*, 914.
[19] E. J. Dil, F. B. Dhieb, A. Ajji, *Polymer* **2019**, *168*, 126.
[20] G. Fredi, M. Karimi Jafari, A. Dorigato, D. N. Bikiaris, R. Checchetto, M. Favaro, R. S. Brusa, A. Pegoretti, *Molecules* **2021**, *26*, 2938.
[21] S. Fakirov, *eXPRESS Polym. Lett.* **2020**, *14*, 436.
[22] S. Fakirov, *Adv. Ind. Eng. Polym. Res.* **2021**, *4*, 187.
[23] P. Nawani, C. Burger, L. Rong, B. S. Hsiao, A. H. Tsou, *Polymer* **2015**, *64*, 19.
[24] A. Asthana, T. Maitra, R. Büchel, M. K. Tiwari, D. Poulikakos, *ACS Appl. Mater. Interfaces* **2014**, *6*, 8859.
[25] X. Su, R. Wang, X. Li, S. Araby, H.-C. Kuan, M. Naeem, J. Ma, *Nano Mater. Sci.* **2022**, *4*, 185.

[26] S. Wu, R. B. Ladani, J. Zhang, E. Bafekrpour, K. Ghorbani, A. P. Mouritz, A. J. Kinloch, C. H. Wang, *Carbon* **2015**, *94*, 607.
[27] M. Tyagi, D. Tyagi, *Int. J. Electron. Electric. Eng.* **2014**, *7*.
[28] K. Chizari, M. Arjmand, Z. Liu, U. Sundararaj, D. Therriault, *Mater. Today Commun.* **2017**, *11*, 112.
[29] P. H. C. Camargo, K. G. Satyanarayana, F. Wypych, *Mater. Res.* **2009**, *12*.
[30] K. Sushmita, G. Madras, S. Bose, *ACS Appl. Mater. Interfaces* **2020**, *5*, 4705.
[31] L. Ma, M. Hamidinejad, B. Zhao, C. Liang, C. B. Park, *Nanomicro Lett.* **2022**, *14*, 19.
[32] N. Saini, K. Awasthi, *Sep. Purif. Technol.* **2022**, *282*, 120029.
[33] A. Saikia, B. R. Bora, P. Ghosh, D. J. Deuri, A. Baruah, in *Nanotechnology in the Life Sciences*, Springer, New York, **2022**.
[34] Q. Fang, K. Lafdi, *Nano Express* **2021**, *2*, 010019.
[35] V. Ganesan, A. Jayaraman, *Soft Matter* **2014**, *10*, 13.
[36] J. Liu, W.-J. Boo, A. Clearfield, H.-J. Sue, *Mater. Manuf. Process.* **2006**, *21*, 143.
[37] T. Khan, M. S. Irfan, M. Ali, Y. Dong, S. Ramakrishna, R. Umer, *Carbon* **2021**, *176*, 602.
[38] A. Alipour, T. Giffney, R. Lin, K. Jayaraman, *eXPRESS Polym. Lett.* **2021**, *15*, 541.
[39] B.-C. Serban, C. Cobianu, N. Dumbravescu, O. Buiu, M. Bumbac, C. M. Nicolescu, C. Cobianu, M. Brezeanu, C. Pachiu, M. Serbanescu, *Sensors* **2021**, *21*, 1435.
[40] R. Mishra, M. K. Aswathi, S. Thomas, High Performance Flooring Materials from Recycled Rubber, **2019**, Ch. 7.
[41] R. K. Mishra, H. J. Maria, K. Joseph, S. Thomas, in *Composites Science and Engineering*, Woodhead Publishing, Cambridge, **2013**.
[42] A. R. Boccaccini, M. Erol, W. J. Stark, D. Mohn, Z. Hong, J. F. Mano, *Compos. Sci. Technol.* **2010**, *70*, 1764.
[43] L. Guo, W. Yuan, Z. Lu, C. M. Li, *Colloids Surf. A: Physicochem. Eng. Asp.* **2013**, *439*, 69.
[44] S. Sarkar, E. Guibal, F. Quignard, A. K. Sengupta, *J. Nanopart. Res.* **2012**, *14*, 715.
[45] A. Kumar, D. Ahmad, K. Patra, *J. Phys. Conf. Ser.* **2019**, *1240*, 012049.
[46] F. Shahzad, P. Kumar, S. Yu, S. Lee, Y.-H. Kim, S. M. Hong, C. M. Koo, *J. Mater. Chem. C Mater.* **2015**, *3*, 9802.
[47] S. K. Ghosh, T. K. Das, S. Ganguly, S. Paul, K. Nath, A. Katheria, T. Ghosh, S. Nath Chowdhury, N. C. Das, *Compos. Part A: Appl. Sci. Manuf.* **2022**, *161*, 107118.
[48] A. Katheria, P. Das, S. Paul, K. Nath, S. K. Ghosh, N. C. Das, *Polym. Compos.* **2023**, *44*, 1603.
[49] S. K. Ghosh, T. K. Das, S. Ghosh, S. Remanan, K. Nath, P. Das, N. C. Das, *Compos. Sci. Technol.* **2021**, *210*, 108800.
[50] S. K. Ghosh, K. Nath, S. Nath Chowdhury, S. Paul, T. Ghosh, A. Katheria, P. Das, N. C. Das, *Chem. Eng. J. Adv.* **2023**, *15*, 100505.
[51] J. A. Song, C. Y. Choi, H.-S. Park, *Comp. Biochem. Physiol., Part C: Toxicol. Pharmacol.* **2020**, *236*, 108801.
[52] J. Sun, Y. Wang, Y. He, J. Liu, L. Xu, Z. Zeng, Y. Song, J. Qiu, Z. Huang, L. Cui, *Carbohydr. Polym.* **2022**, *298*, 120059.
[53] Y. Byun, Y. Zhang, X. Geng, in *Innovations in Food Packaging: Second Edition*, Academic Press, New York, **2013**, Ch. 5.
[54] M. Hara, in *Polymer Morphology: Principles, Characterization, and Processing*, Wiley, Weinheim, Germany, **2016**, Ch. 18.
[55] E. J. Place, J. F. Kennedy, *Carbohydr. Polym.* **1997**, *34*, 411.
[56] L. Mandelkern, *Polym. J.* **1985**, *17*, 337.
[57] Y. Ide, Z. Ophir, *Polym. Eng. Sci.* **1983**, *23*, 261.
[58] V. S. Mironov, J. K. Kim, M. Park, S. Lim, W. K. Cho, *Polym. Test.* **2007**, *26*, 547.
[59] J.-H. Kang, S.-H. Lee, H. Ruh, K.-M. Yu, *J. Electr. Eng. Technol.* **2021**, *16*, 2265.
[60] J.-H. Kang, S.-H. Lee, K.-M. Yu, *J. Electr. Eng. Technol.* **2017**, *12*, 1314.
[61] J. M. Smith, M. State, H. Patrol, J. City, Polarized light microscope examinations of oriented polymer films, Pstc, **2006**.
[62] C. Leyva-Porras, P. Cruz-Alcantar, V. Espinosa-Solís, E. Martínez-Guerra, C. I. Piñón-Balderrama, I. Compean Martínez, M. Z. Saavedra-Leos, *Polymers* **2020**, *12*, 5.
[63] T. Adibaskoro, M. Makowska, A. Rinta-Paavola, S. Fortino, S. Hostikka, *Fire Technol.* **2021**, *57*, 2451.
[64] Z. Jiang, S. Tie, *Trans. Chin. Soc. Agric. Eng.* **2016**, *32*, 209.
[65] J. Liu, H. Liang, *Polym. Bull.* **2022**, *79*, 7923.
[66] Standard Test Method for Tensile Properties of Thin Plastic Sheeting, ASTM International, ASTM **2018**, D882.
[67] N. Oinonen, C. Xu, B. Alldritt, F. F. Canova, F. Urtev, S. Cai, O. Krejčí, J. Kannala, P. Liljeroth, A. S. Foster, *ACS Nano* **2022**, *16*, 89.
[68] S. Thomas, R. Thomas, A. Zachariah, R. K. Mishra, in *Microscopy Methods in Nanomaterials Characterization*, Elsevier, New York, **2017**.
[69] R. K. Mishra, M. G. Thomas, J. Abraham, K. Joseph, S. Thomas, in *Advanced Materials for Electromagnetic Shielding: Fundamentals, Properties, and Applications*, Wiley, Weinheim, Germany, **2018**, Ch. 15.
[70] R. K. Mishra, A. Dutta, P. Mishra, S. Thomas, *Advanced Materials for Electromagnetic Shielding: Fundamentals, Properties, and Applications*, Wiley, Weinheim, Germany, **2018**, Ch. 7.
[71] V. Hondros, M. Vincent, L. Freire, S. A. E. Boyer, J.-M. Haudin, V. Royer, G. François, L. Ville, *Int. Polym. Process.* **2018**, 397.
[72] C. A. Kelly, M. J. Jenkins, *Polym. J.* **2022**, *54*, 249.
[73] B. Patanair, S. Thomas, V. K. Abitha, A. Saiter-Fourcin, *J. Appl. Polym. Sci.* **2021**, *138*, 49838.
[74] S. T. Nair, P. Vijayan P, S. C. George, N. Kalarikkal, S. Thomas, *New J. Chem.* **2021**, *45*, 4963.
[75] S. Thomas, C. Sarathchandran, N. Chandran, in *Rheology of polymer blends and nanocomposites: Theory, modelling and applications*, Elsevier Science, Oxford, **2019**, 19.
[76] J. Abraham, A. P. Mohammed, M. P. Ajith Kumar, S. C. George, S. Thomas, in *Characterization of Nanomaterials*, Elsevier, New York, **2018**.
[77] C. J. Chirayil, J. Joy, L. Mathew, J. Koetz, S. Thomas, *Ind. Crops Prod.* **2014**, *56*, 246.
[78] A. Aldegheishem, M. Aldeeb, K. Al-Ahdal, M. Helmi, E. I. Alsagob, *Polymers* **2021**, *13*, 3083.
[79] J. C. H. Affdl, J. L. Kardos, *Polym. Eng. Sci.* **1976**, *16*, 344.
[80] Y.-B. Park, P. Nardi, X. Li, H. A. Atwater, *J. Appl. Phys.* **2005**, *97*, 074311.
[81] C. Feng, Y. Wang, S. Kitipornchai, J. Yang, *Polymers* **2017**, *9*, 532.
[82] E. Giner, A. Vercher, M. Marco, C. Arango, *Compos. Struct.* **2015**, *124*, 402.
[83] M. M. Shokrieh, H. Moshrefzadeh-Sani, *Polymer* **2016**, *106*, 14.
[84] Y. Akinbade, K. A. Harries, *Constr. Build. Mater.* **2021**, *267*, 120955.
[85] Y.-J. You, J.-H. Kim, K.-T. Park, D.-W. Seo, T.-H. Lee, *Polymers* **2017**, *9*, 682.
[86] M. W. Tham, M. N. Fazita, H. A. Khalil, N. Z. M. Zuhudi, M. Jaafar, S. Rizal, M. M. Haafiz, *J. Reinf. Plast. Compos.* **2019**, *38*, 211.
[87] D. Bousa, J. Luxa, D. Sedmidubský, S. Huber, O. Jankovský, M. Pumera, Z. Sofer, *RSC Adv.* **2016**, *6*, 6475.
[88] A. Vesel, J. Kovac, G. Primc, I. Junkar, M. Mozetic, *Materials* **2016**, *9*, 95.
[89] S. Sharma, A. Paliwal, M. Tomar, F. Singh, N. K. Puri, V. Gupta, *J. Mater. Sci.* **2016**, *51*, 4055.
[90] R. K. Mishra, A. Sabu, S. K. Tiwari, *J. Saudi Chem. Soc.* **2018**, *22*, 949.
[91] S. Singh, V. K. Srivastava, R. Prakash, *Appl. Nanosci.* **2015**, *5*, 305.
[92] S. M. Panamoottil, P. Potschke, R. J. T. Lin, D. Bhattacharyya, S. Fakirov, *eXPRESS Polym. Lett.* **2013**, *7*, 607.